An Analytical Approach to Improve Peristaltic Locomotion of Soft, Earthworm-Inspired Robots in Flexible Soil Media

by

Easton Andrew Foreman

A thesis submitted to the Graduate Faculty of
Auburn University
in partial fulfillment of the
requirements for the Degree of
Master of Science

Auburn, Alabama
May 2, 2026

Keywords: Burrowing robots, Worm robots, Peristaltic locomotion, Soil-structure interaction, Non-linear soil behavior, Cylindrical cavity expansion

Approved by

Ali Khosravi (Chair), Ph.D., P.E., Assistant Professor, Department of Civil and Environmental Engineering, Auburn University

J. Brian Anderson, Ph.D., P.E., Professor, Department of Civil and Environmental Engineering, Auburn University

Paolo Celli, Assistant Professor, Department of Civil Engineering, Stony Brook University

Abstract

Bio-inspired geotechnics is the fast-growing, multidisciplinary field of solving geotechnical-related problems through mechanisms and processes found in nature, development of the technologies requiring input from an array of engineers and scientists. These solutions, such as those within the realm of robotics, are swiftly emerging as a viable candidate for replacing today's underground machinery, offering energy-efficient, cost-effective alternatives paired with minimal ground disturbance compared to conventional industry standards used in subsurface exploration. Though many benefits of employing bio-inspired technology exist, the effectiveness of bio-inspired technologies functioning within real-world soil media is yet to be fully explored. Consequently, this study explored such through a soft, earthworm-inspired robot progressing within simulated soil media through utilizing peristaltic locomotion pathways. Originally developed as a peristaltic robot locomoting through rigid media by Daltorio et al. (2013), work here expanded on these developments by incorporating a simplified analytical framework which was adopted using a sub-structure approach based on soil–structure interaction (SSI) theory to improve the rigid media to one of real-word conditions in which this technology will operate. The surrounding soil was modeled using a system of independent mass-springs, which is a more appropriate alternative than rigid media in capturing compression, rebound, and deformability properties of real-world soil media. Values and calculations representing such parameters were obtained through use of ASCEND (Applications for Spherical and Cylindrical Cavity Expansion in Nonlinearly Deforming Geomaterials), a cavity expansion analysis program developed by Jaeger (2018) capable of simulating cylindrical cavity expansion across a variety of soil types, densities, consolidation histories, and drainage conditions. Results from analytical simulations

yielded details in robot locomotion performance, specifically less-dense soils providing more energy-efficient results in normal force reduction and cost of transport, while higher density and consolidated soils provided robots greater anchorage and thrust capabilities. This study offered promising routes for future research into the field of bio-inspired robotics, providing a comparison evaluation of technology performance across many forms of soil proving useful in selecting burrowing mediums in experimental studies.

Artificial Intelligence (AI) Use Disclosure Statement

In the preparation of this thesis, no Artificial Intelligence (AI) tools were used.

Digital Accessibility Disclosure

In the preparation of this thesis, the following digital accessibility tools were used to ensure this document complies with federal requirements: text alternatives for images that provide clear, descriptive alternative text for all images and non-text content, keyboard accessibility to ensure that all interactive elements, such as hyperlinks, tables of contents, or references, can be accessed and navigated using only the keyboard, color usage to avoid solely relying on color to convey meaning, proper document structure to organize content clearly, contrast to ensure that text has a sufficient contrast against the background, text resizing greater than 200% without loss of content functionality, navigation and headings use of clear and consistent heading to help users quickly find sections of interest, easy to follow navigation, and consistent identification to ensure that elements are clearly and consistently labeled throughout this document for accurate prediction of the action those of such will trigger. The author acknowledges full responsibility for the intellectual content of this work and has made a good faith effort to comply with digital accessibility requirements in publishing, wherein the nature of the content does not significantly change in order to do so. Furthermore, all content has been reviewed and revised to meet these requirements prior to final publication.

Acknowledgments

I dedicate this thesis to my family, who have spent the better part of 6 years supporting my scholastic endeavors. You are my biggest pillar of support not only in academics, but in life. Thank you for your guidance through times both good and bad.

To my parents, Lisa and Brent Foreman, your drive and pursuit of excellence is my daily motivation to always do my best. From a young age, I knew I wanted to do something great with my life. I believe you knew this too, your steadfast support empowering me to achieve both an undergraduate and graduate degree in engineering from Auburn University. You made these accomplishments possible through teaching great habits, a strong work ethic, and best of all, instilling a love for doing difficult things. I am so proud to be your son.

To my brothers, Evan and Ethan, our camaraderie surely pulled me through difficult times in school. From familiar conversations, to offering advice on difficult circumstances, our brotherhood gave me much confidence in my abilities in my field of study. Best of all, our love for Auburn University and engineering kept my mind focused on education at the school we have supported all our lives. You shaped this period of my life into one I reflect on fondly - from starting my Auburn journey as your roommate, to technical conversations between class and our early careers, you made everything worth it. War Eagle, and thank you both.

Lastly, to my fellow students in our research group, Hamid Reza Tohid Vand and Qin He, thank you for your friendship during my Master's journey. You made long hours in the laboratory enjoyable and provided a light-hearted atmosphere for someone new to research. Your technical support on this project, willingness to help me succeed, and the long hours lending aid building prototypes will not be forgotten. I appreciate your sacrifices in helping me succeed.

Table of Contents

List of Tables

List of Figures

List of Abbreviations

CPT…Cone Penetration Test

FEA…Finite Element Analysis

STEM…Science, Technology, Mathematics, Engineering

FEM…Finite Element Modeling

SSI…Soil-Structure Interaction

CET…Cavity Expansion Theory

MIT…Massachusetts Institute of Technology

COT…Cost of Transport

ASCEND…Applications for Spherical and Cylindrical Cavity Expansion in Nonlinearly Deforming Geomaterials

SBT…Soil Behavior Type

OCR…Over-Consolidation Ratio

COM…Center of Mass

NFR…Normal Force Reduction

Chapter 1: Introduction

1.1 Project Background

Subsurface exploration is fundamental to various disciplines within engineering and environmental sciences, including geotechnical site characterization, infrastructure development, and environmental monitoring. Conventional techniques for exploration such as excavation, drilling, and boring remain the standard practice for accessing underground strata and collecting soil data. Despite their widespread application, these methods present notable limitations, especially in urban and environmentally sensitive settings. In densely populated areas, the presence of undocumented or poorly mapped underground utilities—such as water mains, gas lines, and electrical conduits—poses significant risks. Accidental damage during intrusive operations can lead to costly repairs, service interruptions, and safety hazards (Norby et al., 2024; Alqadad et al., 2017). Continuing, traditional machinery requires considerable working space, introduces noise and vibration, and often disturbs local ground and structures leading to resistance from surrounding communities. These impacts are even more pronounced in ecologically fragile zones. Furthermore, high operational costs, logistical challenges, and the need for specialized labor further restrict the deployment of conventional methods in complex or remote environments where space and resources are limited. It is for these reasons that traditional subsurface exploration methods are not suitable and unsustainable in particular circumstances, possessing numerous limitations. Observations of these mechanisms are assisting in improving common field tests carried out by smaller, less powerful drilling rigs (such as CPT tests) that may not provide an adequate amount of reaction force necessary for in-situ site investigations at limited-access project sites, which can include testing at greater depths, dense soils, and perhaps extreme environments.

In a variety of circumstances, traditional methods used to perform subsurface exploration expose great risk of damage to surroundings and the environment, injury, and require vast energy consumption to drive processes, among others. Fortunately, alternative technology, such as those within the realm of robotics, is swiftly emerging as a viable candidate for replacing today's underground machinery. Robots are capable of not only being remotely manipulated and controlled, but performing tasks autonomously, effectively eliminating risk to operators while pushing the boundaries of possibilities in subsurface environments considered "extreme" by human standards. Furthermore, the size, shape, and morphologies of robots are much smaller in comparison than traditional subsurface machinery, their weight being a small fraction, all reducing cost of mobilization, cutting expense towards malfunction, and significantly lowering the risk of infrastructural and environmental degradation. Lastly, robots can be designed to accomplish virtually any task granted the engineer equips such technology with the appropriate means to do so. Shapes, morphologies, even the movement mechanisms of technology are thoughtfully designed to situate robots in the best position for accomplishing tasks set forth in energy-efficient, non-destructive pathways. Often, such morphologies and mechanisms contributing to the design of the technology's size and shape are inspired from those already present in our world, namely those existing within nature, dubbed "biological inspiration". Identifying shapes, sizes relating to morphology, as well as mechanisms, both inspired from biology and furthermore evidenced in accomplishing similar tasks to that of which is at hand means narrowing the scope of study and simplifying design criteria. Fig. 1.1 shows a physical concept of a soft, earthworm-inspired robot, comparing its morphology and mechanisms to burrowing earthworms in the subsurface.

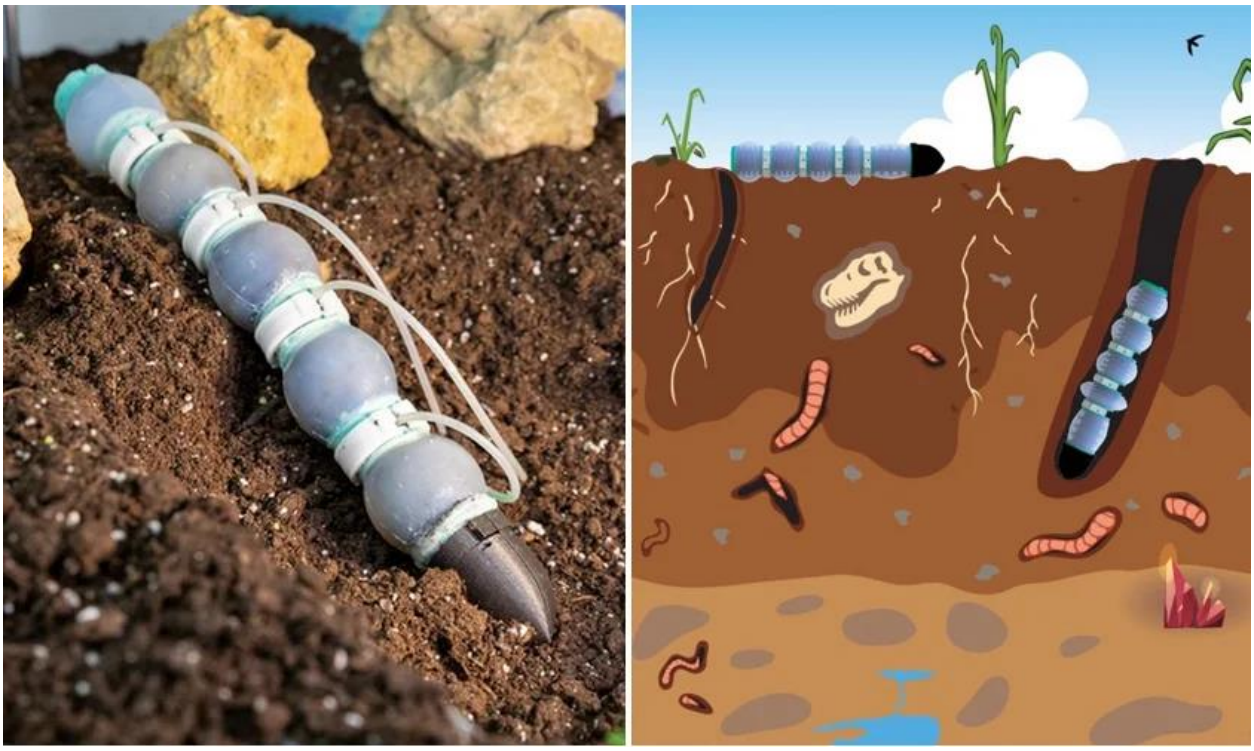

Fig. 1.1. Physical concept of a subsurface robot inspired by morphology and mechanisms of earthworms (CIO Bulletin, 2023).

Earthworms have emerged as a viable candidate to use as a model for robot locomotion. Various sections belonging to the earthworm aid in their burrowing capabilities. Non-moving segments (those that are fully dilated) are prevented from slipping backward by use of small setae located on the body, which are used to anchor and prevent expanded segments from slipping backward while segments in front lengthen to achieve forward progression (Alexander, 1982). The anterior end then continues the process by shortening and radially expanding, which acts to lengthen the burrow hole by crack extension before the head alternates back to lengthening and radially contracting to reach the front of the burrow hole once again, all followed by a wave-like motion down the body known as “retrograde peristalsis” (Dorgan, 2018). This form of movement progresses the earthworm further into the media and continues the burrowing process while the posterior end is dragged deeper into the burrow (Seymour, 1971). Furthermore, the flexible,

compliant bodies of earthworms enable them to conform to the surrounding environment, minimizing ground disturbance and the risk of damaging buried infrastructure, while also allowing for normal forces to be applied isotropically to the cavity walls in radially expanded segments in the peristaltic process (Martinez et al., 2020; Tang et al., 2025). Fig. 1.2 shows the combination of muscles working antagonistically, enabling the soft earthworm to perform peristaltic locomotion.

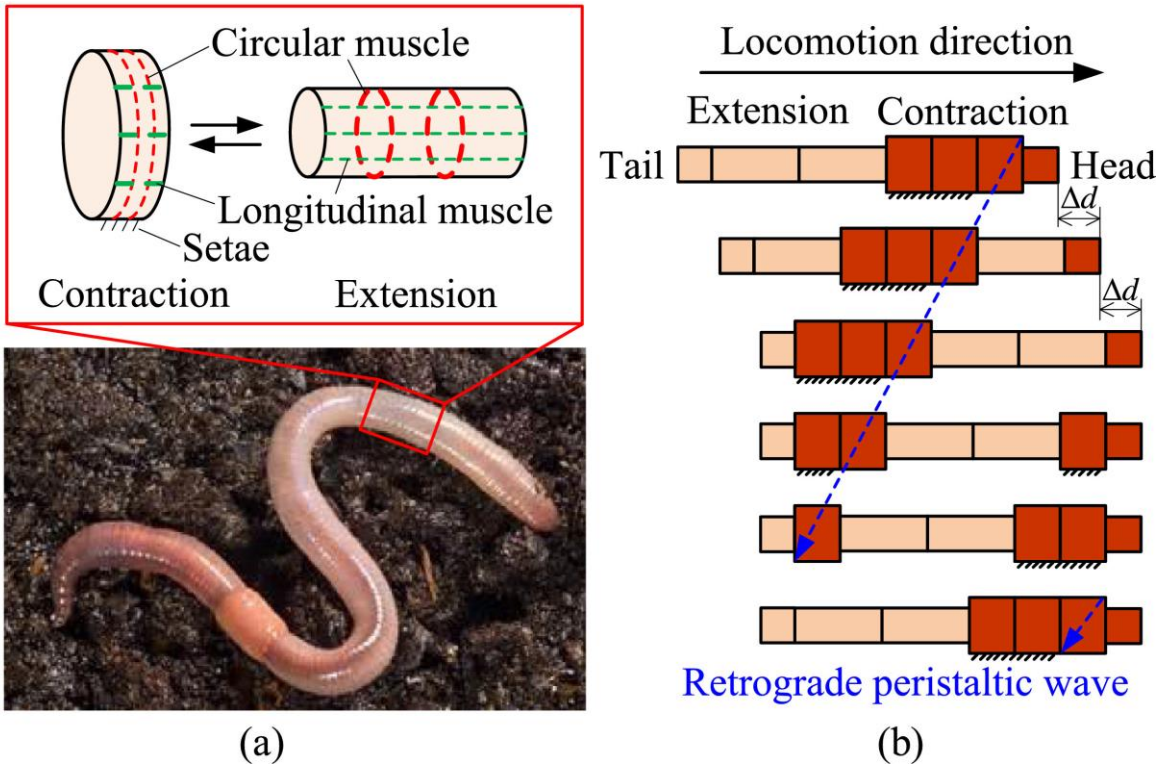

Fig. 1.2. Morphology and depiction of locomotion process in earthworms, a.) earthworm muscular structure, and b.) mechanism of locomotion relative to direction of movement (Liu and Yao, 2019).

Inspired by earthworms by their non-destructive locomotion pathways and compliance to stress, soft robotic systems have emerged as a promising alternative to traditional rigid machinery for subsurface operations, particularly where ground disturbance, surface disruption, or proximity to existing infrastructure must be minimalized. This need is especially acute in urban

environments, where an expanding network of underground utilities increases the risk of service disruptions during traditional earth-related work. Recent experimental efforts have aimed to replicate the biomechanics of earthworms to improve the mobility of soft robotic systems in underground environments. Soft robots such as these have the advantage of flexibility and fluid-like movements found in the earthworm while also possessing the ability to exert extraordinary amounts of pressure in underground environments, a key requirement in anchorage and generation of thrust force that life below ground surface must be capable of performing in order to locomote. Additionally, robots inspired by the nature of biological processes possess modular design, energy-efficient actuation, and a potential for autonomous operation make them well-suited for long-term deployment in both urban and natural settings. As a result, earthworm-inspired soft robots have emerged as promising, non-invasive technology for subsurface exploration and monitoring (Milana, 2022; Le et al., 2025).

Other soft robots exist containing designs inspired by mechanisms and phenomenon depicted in biology and nature as well, created for soil investigations and civil engineering applications similar to earthworm-inspired robots. A plant root-inspired soft robot, developed to mimic the pathways of plant root navigation and pressures they are capable of exerting, is excellent for studying natural steering and control around objects requiring high pressures instantaneously to burrow through. Another form of soft robots, designed from the morphology and mechanisms of the Atlantic Razor Clam *E. directus*, incorporates the clam's ability to perform "deep" burrowing through local substrate-modifying pathways (Winter et al., 2014). By developing soft, mechanical members internally inspired by those belonging to the clam, mechanisms are carried out that perform identically to the Atlantic Razor Clam, thus providing instant usefulness to subsurface engineering applications. Both robots here have instant positive impacts on

underground investigations but come with considerable drawbacks compared to earthworm-inspired robots. Plant root-inspired robots are limited to slow locomotion speeds, a hinderance to project deadlines and otherwise urgent situations. In clam-inspired robots, burrowing direction is limited to the vertical direction, and furthermore, cannot incorporate steering or turning due to morphological and anatomical constraints. Earthworm-inspired robots, however somewhat limited by soil type, overcome these challenges at greater ease. Soft worm robots possess strong internal structures, which allow the robot to "push" tougher subsurface materials (such as rock) aside during locomotion, whereas plant root-inspired robots would need to navigate around those. Earthworm-inspired robots also possess the unique ability of not only horizontal burrowing but also access limited vertical burrowing directions through steering mechanisms. Soft, earthworm robots are unique in their capabilities and offer promise for full autonomy compared to soft robots inspired by other biological morphologies. Fig. 1.3 depicts example concepts of other bio-inspired robots and their mechanisms for locomotion. Fig. 1.3 (a) shows a plant root-inspired robot with side comparison of a real plant root (Sadeghi et al., 2014), while Fig. 1.3 (b) shows A robot inspired by the Atlantic Razor Clam, which is depicted in chronological phases performing its locomotion mechanism for vertical advancement (Winter et al., 2014; Wei et al., 2021).

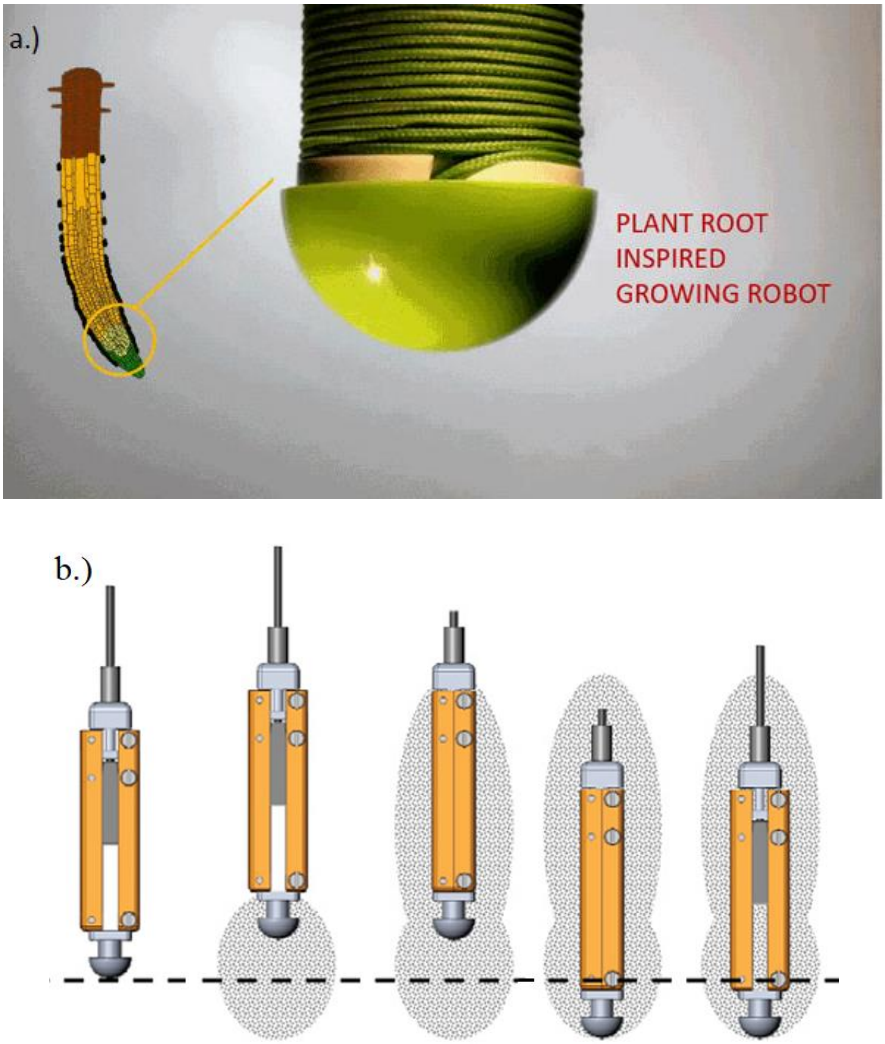

Fig. 1.3. Different soft robots used for subsurface investigations, a.) a plant root-inspired robot (Sadeghi et al., 2014), b.) A robot inspired by the Atlantic Razor Clam (Winter et al., 2014) .

Of course, the design of soft, undergrounding robots is not a simple endeavor. The task requires expertise from a vast array of professions – many disciplines of engineers, scientists, and technologists, to name a few, making the field of biological-inspired technology, or bio-inspired robotics, a highly interdisciplinary field of study. Geotechnical engineers are certainly included in this space, possessing a great deal of knowledge on soil mechanics and in-situ conditions relevant to the environments in which subsurface, soft robots are interacting with. Geotechnical expertise is indeed valuable in the study of soft robots, and specific tools and analyses exist in which such

research is carried out. One tool in particular, which is relevant to this work, is the employment of finite element analysis (FEA). FEA, which is a form of computer modeling, is a numerical simulation technique employed by many professionals in STEM careers, which is employed to determine how an object interacts with real-world forces and physical effects (Fadiji et al., 2018). FEA simulations, in this case, allow studies on robot interactions with projected environments to be conducted, in which professionals are thus enabled to analyze performance of the robot, including if part(s) function as intended, malfunctions, and others. In some cases, modeling using finite element analysis (FEM) is conducted as parts of major studies, while others, it is a tool employed for simple verification purposes. Environments, the object of study, or both, can be reduced to simple forms in order to unmistakenly determine if results from external studies align with those retrieved from these numerical simulations. Relevant to this study, example simulations may include simulating overburden pressures of high magnitude, varying dimensions/geometry/minor details of soft robots, even various properties pertaining to those of elastomeric and steel may be studied using FEM, drawing on the appeal of the tool's convenience. It is a complicated, yet powerful analysis utilized by a wealth of researchers in order to obtain accurate results from advanced studies, saving expenses and time if otherwise physically conducted in experiments. Fig. 1.4 illustrates example FEM results of a segment behaving comparably to earthworm body segments during simulations of peristaltic locomotion, Fig. 1.4 (a) representing an actuator controlling radial movements and Fig. 1.4 (b) representing an actuator controlling axial movements (Li et al., 2024).

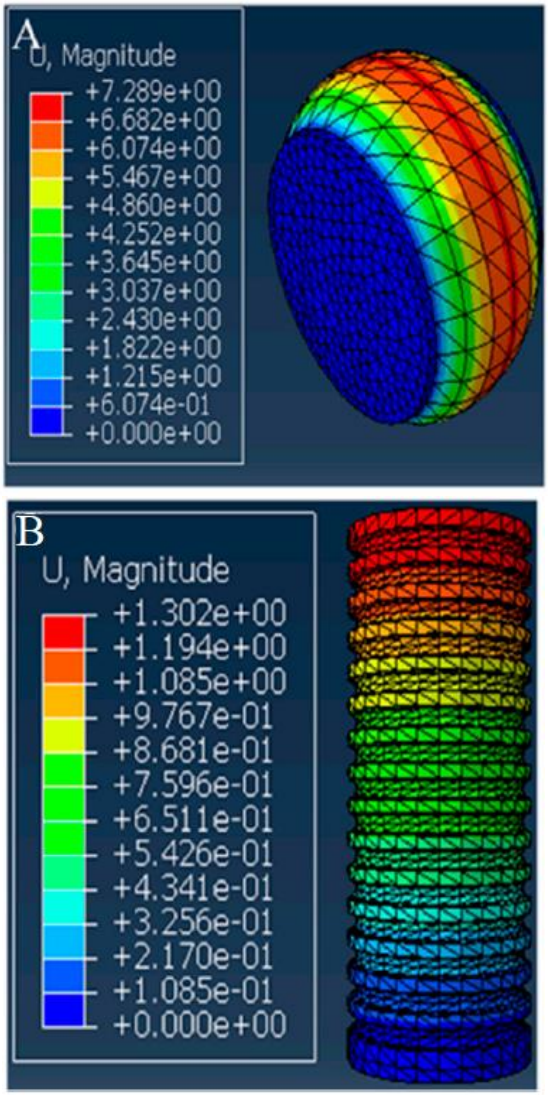

Fig. 1.4. Numerical simulation example results, a.) Simulation results of an actuator controlling radial movements (Li et al., 2024), b.) Simulation results of an actuator controlling axial movements. (Li et al., 2024)

1.2 Research Objectives

The aim of this study is to establish a computationally efficient analytical approach to accurately predict the effects of a peristaltic, earthworm-inspired robot locomoting through deformable soil media that accounts for soil-structure interaction (SSI) concepts. Given this, the objectives of this study included:

- Characterize magnitudes of forces and displacements derived from interactions between an analytically simulated, peristaltic robot and linear-elastic, deformable soil media.
- Analyze magnitudes of forces and displacements between analytically simulated peristaltic robot of various lengths and deformable soil media exhibiting a non-linear, force-displacement relationship.
- Perform parametric study and comparative analysis of soil behaviors, reaction forces, and pressures exerted from local soil of various classifications, densities, and stress histories in response to robot segment expansion.
- Verify results of peristaltic burrowing robot analytical model through finite element analysis (FEA)

1.3 Scope of Work

The scope of work is centered on development of a computationally efficient analytical method for modeling peristaltic locomotion of an earthworm-inspired robot in deformable soil media. Of primary focus is incorporation of soil-structure interaction (SSI) concepts into robot and soil interactions. The scope of this work included the following:

- Develop an analytical model of robot-scale peristaltic locomotion that describes the paired actions of radial expansion/axial shortenings and radial contraction/axial elongation within simulated soil media
- Incorporate soil-structure interaction (SSI) to account for essential behaviors in soil mechanics that govern performance of peristaltic locomotion, including:
    - Anchorage and slip of contacting segments
    - Stress redistribution around radially expanding segments
    - Elastic and elasto-plastic soil response

- Analysis of energy expenditure and locomotion performance, where the analytical model becomes a tool to evaluate:
    - Propulsion system and thrust generation
    - Segment anchoring stability
    - Energetic cost of locomotion
- Parametrically characterize and comparatively assess soils, properties, and conditions notably affecting efficiencies of peristaltic robot burrowing.

Chapter 2: Literature Review

2.1 General Background

Through history, various technological developments have been modeled from the morphology, functions, and abilities of biological organisms. Particularly, in the realm of self-burrowing robots, locomotion has taken inspiration from that of biology (such as vermiform, peristaltic locomotion of earthworms, or the penetrating processes of plant roots), which seeks to merge the fields of biotechnology and geotechnics into one fast-growing, interdisciplinary sector of engineering, known as bioinspired geotechnics (Tang & Tao, 2021; Jain et al., 2023). This field is broadly defined as the application of biological strategies to solve geotechnical and soil-related engineering problems. Biologically inspired methods have swiftly become a promising approach for autonomous undergrounding robots since before the 21st century, offering ecologically friendly, energy-efficient mechanisms to model robot movement after that minimizes disturbance of local soil regions (Gaymer, 1971; Meyers & Guillot, 2007). Saga et al. (2016) applied reinforcement learning techniques, specifically the Actor–Critic algorithm, to optimize segment coordination of a multi-segment peristaltic robot. Their results demonstrated the feasibility of autonomous navigation in confined environments, underscoring the potential of peristaltic crawling for post-disaster search and rescue operations. In addition to physical prototyping, numerical modeling has played a crucial role in advancing the design and analysis of soft robots. Planar dynamic models, such as those proposed by Bi et al. (2023), have enhanced understanding of segmental coordination and force transmission, providing insights into locomotion in complex terrains. Finite Element Analysis (FEA) has been used to predict stress distributions and deformation behaviors in soft actuators, while Discrete Element Method (DEM) simulations have been instrumental in capturing the granular interactions between soft robots and soil. For instance,

Tang and Tao (2022) employed DEM to analyze the effects of rotation on penetration resistance in sandy soils, revealing that rotational motion can significantly reduce contact forces and energy consumption, a finding with direct implications for robotic burrowing strategies.

By recreating the same means to achieve a similar result, these biologically inspired mechanisms can be ideal for locomoting robots through small and narrow spaces (Daltorio et al., 2013). For example, Ge et al. (2017) introduced a pneumatically actuated soft robot capable of bidirectional locomotion, leveraging variable surface friction to simulate muscle contraction and earthworm anchoring mechanisms. When mimicking burrowing behavior of biological organisms, acknowledgment of the existence of a dynamic relationship between the burrowing organism and the burrowing cavity means incorporating vast theories to accurately compute and characterize expanding interactions between the soil, embedded structure, and processes conducted when cavities expand in the subsurface. The issue with advancing self-penetrating robot technology lays incident in that very setting; while this dynamic relationship has been explored, practitioners have yet to perfect and fully replicate robotic burrowing in the soil domain (Khosravi et al., 2018). Furthermore, the energy terms required for such technology to successfully expand and navigate through a subsurface borehole of various, comparable soil classifications and conditions to complete its designated function within our infrastructure remains to be explored. Autonomous, self-burrowing robots have the potential to contribute much to society: from geotechnical and construction applications, rescue missions through earthquake rubble, even to extra-terrestrial, off-planet exploration missions, these robots can perform tasks us humans simply cannot, and more efficiently than current methods and industry practices (Wengang et al., 2003; Fukunaga et al, 1998)

2.2 Biological Inspiration

Burrowing animals inhabit much of Earth's various substrata, spanning most animal phyla as well as orders of magnitude in size (Dorgan, 2015). Burrowing is a technique utilized by many soft-bodied, elongate animals use to move and is estimated to date back to the Precambrian period, at earliest (Dorgan, 2018). The act of burrowing, which takes place as a mechanical process (Ansell & Nair, 1969), is defined by Dorgan (2015) as movement through soft substrata by grain displacement and is employed by capable biological organisms to traverse the subsurface for habitat exploration, space creation, and search for food. This process can be achieved by many facets of soil deformation fluidization, fracture, compaction, and excavation between small and large animals, where burrowing method largely depends upon animal body size, morphology, and mechanical properties of the soil medium, in no order (Dorgan, 2015).

Subsurface burrowers employ a multitude of behaviors to propel themselves and navigate through a soil medium. Burrowing mechanisms are employed and made possible by the muscular and morphological characteristics belonging to specific biological organism, and those of interest exist within two phyla of the biological taxonomic classification – Annelida and Mollusca. Contained within these are organisms that employ locomotive mechanisms of interest, among others, in the realm of undergrounding robots. Describing the various muscle arrangements and morphological characteristics of interest present in organisms of interest are important when understanding the biological inspiration needed for undergrounding robots, as the presence and arrangements of different features contributes to the organism's method of locomotion. A simple depiction of burrowing muscles and morphologies for different muscle arrangements are given in Fig. 2.1 and 2.2**,** respectively (Wainwright, 1988).

Fig. 2.2 depicts various shape changes in pressurized cylinders, Fig. 2.2 (b) the Orthogonal Muscle Fiber Array (OMFA), Fig. 2.2 (b) the OMFA preventing length change, Fig. 2.2 (c) the OMFA providing stiffness in bending until failure occurs, Fig. 2.2 (d) the OMFA allowing torsion and twisting along the longitudinal axis, Fig. 2.2 (e) The Crossed-Fiber Helical Array (CFHA), Fig. 2.2 (f) CFHA allowing length change, (g) CFHA allowing for bending in smooth curves, and Fig. 2.2 (h) CFHA resisting torsional movement (Wainwright, 1988).

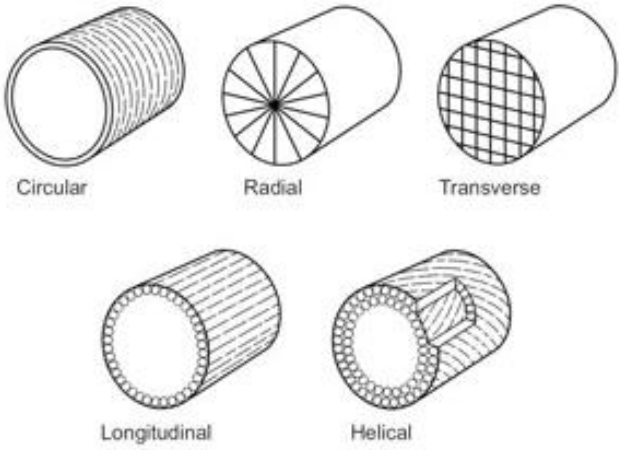

Fig. 2.1. Schematic of common muscle fiber orientations in soft-bodied (Dorgan 2007, Kier 2012, Law et al. 2013)

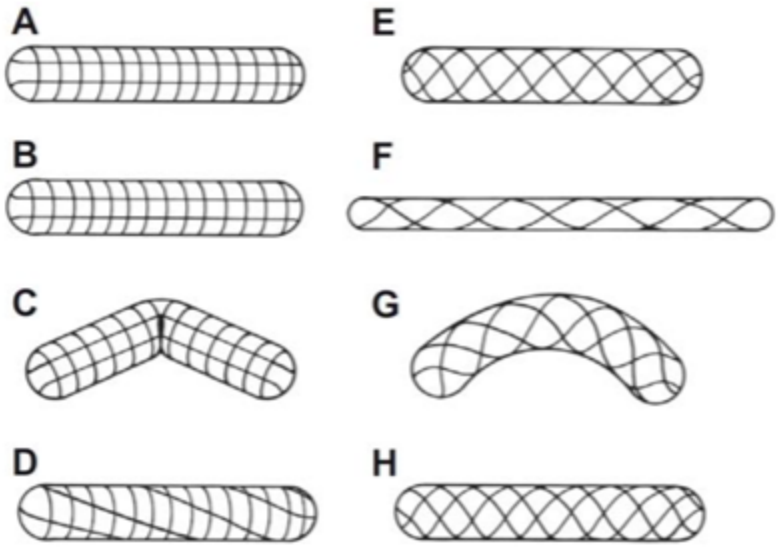

Fig. 2.2. Shape changes in pressurized cylinders, a) Orthogonal Muscle Fiber Array, b) OMFA prevents length change, c) OMFA provides stiffness in bending, d) OMFA allows torsion and twisting, e) Crossed-Fiber Helical Array (CFHA), f) CFHA allows length change, g) CFHA allows for bending, h) CFHA resisting torsion (Wainwright, 1988).

Armandia brevis, a cylindrically shaped, deposit-feeding annelid, utilizes undulatory locomotion to burrow through the shallow subsurface of sandy muds and loose sands (Woodin, 1974; Hermans, 1978). A. brevis lacks particular muscle fibers found in most segmented worms, being circular and longitudinal muscles, therefore differing in the mechanism it must use to locomote compared to other Annelids (Tzetlin and Filippova, 2005; Purschke and Muller, 2006). Undulation is the form of movement characterized as a unilateral contraction of thick longitudinal muscle bands combined with large amplitude “wiggling” movements of its head, to burrow effectively. The European lugworm burrows similarly to other worms, using setae (stiff, bristle-like structures protruding from the body) to increase friction within their burrows as they expand and contract their body to move through sediment. The setae assist by anchoring parts of their body to the burrow walls, allowing them to apply the necessary forces to push forward and progress

through the soil without losing their position (Crane and Merz, 2017). The lugworm also possesses a specialized form of burrowing when burrowing in loose granular materials such as coarse sands. The organism has been observed to pump water into the anterior end of the burrow hole to dislodge grains and soften the soil, locally weakening the soil at the front of the burrow to enable deeper burrowing (Crane and Merz, 2017; Dorgan et al., 2006; Dorgan, 2015). The Atlantic Razor Clam, a bivalve mollusk that is enclosed by two "valves" connected to a hinge positioned axially longitudinal to the animal, uses another method of dual-anchor locomotion. The organism contains a "foot," or pedal, and alternates between a series of movements between its valves and foot to pull itself deeper into the substrate known as the organism's "digging cycle" (Winter et al., 2012 and Trueman et al., 1967). However, this work alone cannot account for the bivalve's ability to burrow to deep depths. Paired with its digging action is another mechanism known as "localized fluidization," which is performed to loosen the sand around the clam and thereby reduce resistance to shell movement and the energy required for burrowing. When the organism ejects water from its mantle cavity, first noticed by Drew (1907), pore water pressure increases in the surrounding soil, reducing effective stress and shear strength, thereby allowing the clam to dig more easily.

Last to discuss within biological burrowing behaviors is a key mechanism for subsurface locomotion of limbless, soft-bodied organisms. Peristalsis, which is a form of vermiform locomotion (Trueman, 1967), is a movement that involves alternating waves of elongation and shortening that move along the body. These waves, combined with differential friction, enable forward movement (Gans 1973, Elder 1980, Dorgan 2018, Summers and O'Reilly 1997). Shortening of the body expands cavities, creating reaction forces that assist in penetration, while elongation reduces contact area and friction, facilitating burrowing (Fager 1964, Trueman 1966, Shin et al. 2002, Dorgan et al. 2005, Jung 2010, Summers and O'Reilly 1997). Peristaltic

locomotion is a coordinated action made possible by circular and longitudinal muscle fibers working antagonistically during locomotion. When one set of muscles contracts, the other must extend. Many annelids utilize peristalsis as a primary or secondary form of locomotion, but of principal focus for this work is the Earthworm (Lumbricus terrestris). Earthworms, belonging to the phylum of annelids, possess cylindrical bodies that are segmented with around 100 to 150 segments, each containing muscles and the same bristle-like structures, setae, common in other worm species discussed previously. Fig. 2.3 shows a schematic of an earthworm and related anatomical features within stages of peristalsis.

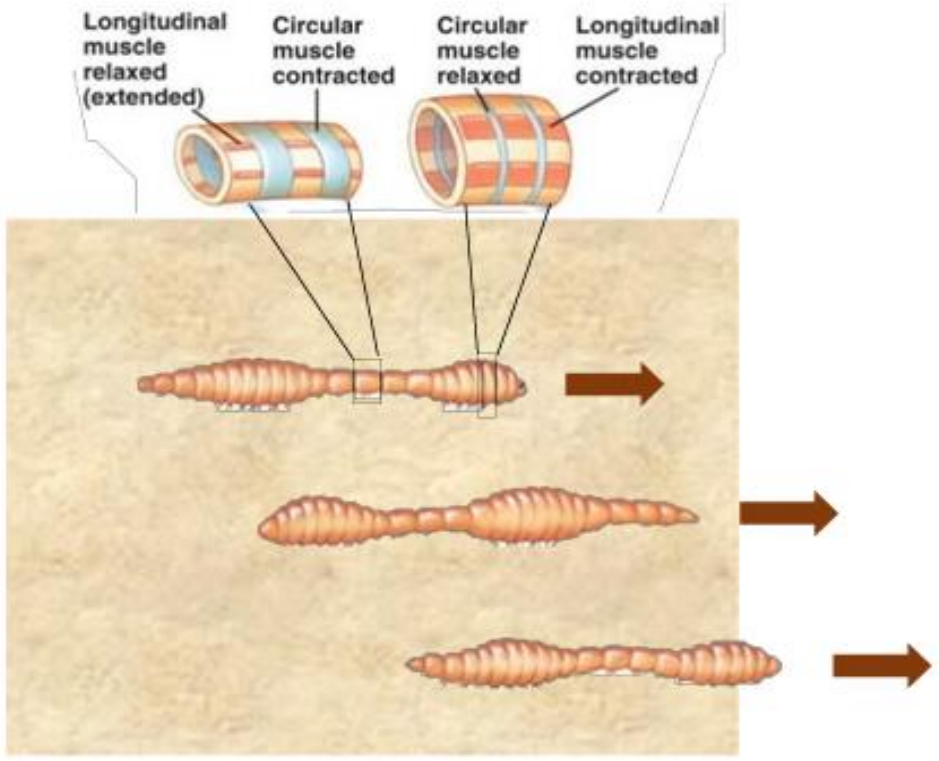

Fig. 2.3. Alternating contractions of the earthworm's circular and longitudinal muscles (Sadava et al., 2009; Kurth and Kier, 2014)

Biological techniques have given inspiration to technical practice, namely that of engineering in and around soil mediums, as the need to create space within solid substrata is

important. Understanding how biological organisms overcome challenges in regular burrowing significantly impacts technological development, as such problems will undoubtedly be encountered on a grander scale.

2.3 Bio-Inspired Geotechnics

The earthworm and its processes are an ideal candidate for inspiration in robot design for a multitude of reasons. To start, the organism's morphology and exterior anatomy are simple to replicate. Other organisms mentioned previously are quite different in size and features, which can create difficulties in many facets of design. The lugworm having different sized anterior, middle, and posterior body sections (Wells, 1950), giving a tapered appearance affecting structural design, the razor clam, a bivalve shell, containing an intricate, connected system of mantle and siphons used for localized fluidization discovered by Drew (1907) and later studied by Winter (2011) requiring a hydraulic aspect and not applicable in unsaturated or dry soils, and lastly, and the lugworm requiring an eversible/expandable anterior appendage, to aid in its burrowing process as well as in certain soils (Crane and Merz, 2017; Dorgan et al., 2006; Dorgan, 2015). The earthworm's morphology is simple to replicate compared to these.

Continuing, the earthworm burrows through all substrates primarily using one mechanism – peristalsis. Having one primary mechanism for locomotion is easier when developing technology design, as such a mechanism is responsible for overcoming the same subsurface challenges, but in a less convoluted process, that other organisms must overcome using paired or combined mechanisms. A. brevis relies heavily on setae and oblique muscles to undulate, making it a weak burrower at depths less close to the surface, the razor clam, without fluidizing the soil, a mechanism difficult to perform in soils that differ from those saturated and cohesionless, can only generate a force capable of burrowing 1 – 2cm into sea beds (Trueman, 1967 and Winter et al.,

2012), while the lugworm requires a combination a various anatomical features to anchor and drive itself forward into saturated substrates (Crane and Merz, 2017). Lastly, the earthworm is a terrestrial burrower, inhabiting dry and unsaturated soils of all classifications and at various depths, though it is noted by Dorgan et al. (2006) that peristalsis is more effective in coarse-grained, less cohesive soils. Other organisms of comparison here mainly inhabit saturated zones, or at extremely shallow depths. Therefore, understanding this information before simulating and designing bio-inspired technology is significant.

A wealth of authors and industry professionals have contributed to the emerging field of bio-inspired geotechnics. These contributions are nested within the category of bio-inspired design, defined as extracting a biological organism's natural solution and applying it to solve a problem in engineering (Martinez et al, 2020). Bio-inspired geotechnics consists of specifically applying such designs and solutions reigning from biological organisms to problems within geotechnical engineering. In the realm of bio-inspired geotechnics, burrowing mechanisms of a variety of sorts have been observed and employed in efforts to achieve greater penetration and locomotion techniques in subsurface geotechnical monitoring, increasing movement efficiencies within mechanisms, among others within the field of study. Tang et al. (2024) designed a soft, vertical and horizontally burrowing robot inspired by plant seed penetration techniques that can decrease penetration resistance in sands using specific movement mechanisms. Inspired by a common mechanism in Caecilians, earthworms, and razor clams involving radially expanding segments while an adjacent segment radially contracts and axially elongates, Khosravi et al. (2018) performed DEM simulations to understand the effect of body geometry during burrowing in development of self-inserting, in-situ testing probes capable of generating their own reaction forces. Realizing the need for improvements in soil investigations in urban, sloped, and forested

areas, Martinez et al. (2019) developed a self-penetrating site characterization probe capable of delivering reaction forces high enough to successfully perform in-situ tests. Where mobilization of smaller rigs is traditionally done to accomplish such tasks that possess the anchoring capabilities to generate necessary reaction forces required for common in-situ tests, the risk of disturbing ground conditions, and therefore, soil samples of the ground being tested, is much higher and therefore negates the purpose of in-situ tests. The bio-inspired technology developed by Martinez et al. (2020) greatly reduces disturbance of local soil in such environments while also maintaining the ability to penetrate challenging soils, such as stiff and dense mediums, thereby increasing the feasibility of performing in-situ tests in challenging environments.

Movement strategies exhibited by specific animal mechanisms in nature have a particular application to development of self-burrowing soft robots modeled after earthworm locomotion. Of particular interest to this work, Daltorio et al. (2013) developed a large, soft bodied, peristaltic worm robot that minimizes slippage to efficiently locomote through rigid pipes of varying radii. Taking inspiration from efficient burrowing mechanisms and appearance of earthworms, this robot mimics and conducts the movement process known as peristalsis. The process is conducted by sequential radial contraction and axial elongation, complimented by radial expansion and axial shortening of adjacent segments along the earthworm's body. As opposed to the body of the earthworm axially lengthening and shortening as a whole, individual body segments perform these tasks independently, occurring successively where each segment slightly changes in length based on the connected segment located anterior or posterior of the segment of interest, to achieve forward propulsion through narrow or deformable media (Alexander, 2013). Where the process begins with lengthening at the anterior end (the head of the earthworm), the following sections alternate by shortening and expanding to produce forward thrust for gradual-lengthening sections

in front. The process continues down the body of the earthworm towards its posterior end, where initial segments contract and are pushed forward followed by increasingly shorter and radially expanded sections.

Equally important in robot design is understanding that smaller organisms utilize different burrowing mechanisms than larger animals, with the latter having the ability to burrow at further depths, typically. Should an undergrounding robot be selected to utilize peristaltic locomotion, though, a process seen in smaller organisms, questions arise regarding obtaining comparable efficiencies in large-scale burrowing that is achieved at earthworm scale. Continuing, peristalsis and small-animal locomotion alike are typically observed closer to the surface, where loading and stress on the soil is not too great for grain displacement. Peristalsis requires a concept known as "fracture" conducted at the anterior tip (head), where grains are then compacted to greater proportions as the worm "makes space" for subsequent peristaltic sections to move through. When addressing the possibility of upscaling the process for larger organisms, in this case, an undergrounding robot, issues arise to assessing required forces necessary to perform peristalsis at the same efficiency as the organisms of inspiration. Action must be taken to assess the interaction between the soil and structure in contact with it, including the soil's response to static loads, moving loads, and expansion forces.

2.4 Soil-Structure Interaction

The foremost concept in any project dealing with a structural system is understanding how it interacts with the foundation and soils (beneath and locally surrounding) area at which are members of the system. One such approach towards this is incorporating soil-structure interaction (SSI) into analysis. Incorporating a dynamic soil-structure analysis of such interactions between the structure, or the superstructure, and the foundation and surrounding soils, or the substructure,

means to measure how the systems react to ground excitation when considered as a whole unit to events such as earthquakes and has significant recourse on the structural response due to such excitation (Abdulaziz et al., 2022; Kutanis & Elmas, 1999). SSI typically takes an iterative approach and reduces seismic needs within structural design (FEMA P-2091). According to Abdulaziz et al. (2022), SSI measures how the superstructure and the substructure (foundation, surrounding soils) collectively react to a free-field ground motion, a concept describing motion that is unaffected by wave scattering, structural, and foundational vibrations. If a stiff foundation is resting on a rigid soil block, SSI effects are not applicable.

If SSI is not appropriate for problems involving rigid materials, then it can be inferred that the analysis is only valid for materials and mediums that are flexible in nature. Bio-inspired robots and the environments in which they locomote satisfy this condition quite well. Pertaining to this work, Daltorio et al.'s (2013) peristaltic robot "Softworm," the physical robot (superstructure), which is the testing prototype for burrowing simulations in their work, provides adequate stiffness to distribute the ground reaction forces based on variation in mesh diameter but is made up of continuously deformable mesh that is still compliant under load. The burrowing environment (substructure), in this case, simulated soil media, is deformable by definition and application of SSI. To start, when considering the interaction between soil and a structure from the perspective of undergrounding robots, the problem must begin by considering them as both 1.) a simplified case, and 2.) a discrete case. Most common interactions are imagined as a structure with a foundation interacting with the surrounding soil (FEMA P-2091). Fig. 2.4 depicts a simple example schematic of SSI modeling. In a simple analysis of an SSI model, the structure is modeled using nodes to represent its boundaries, both outside of the substructure and within it, signifying the interface between the superstructure and unbounded, free-field substructure. Those same nodes

can be used to model the unbounded substructure with the superstructure excavation in place. The soil wedge where the structure is embedded in the unbounded soil. Using this same node system, the soil wedge representing the embedded superstructure can be obtained. These give us a simple, partitioned model of the free-field with nodes of the excavation in place, in the location of where the structure, giving valuable information on the excavated wedge's response to free-field excitation which, as previously described, is key in any conducting SSI analysis.

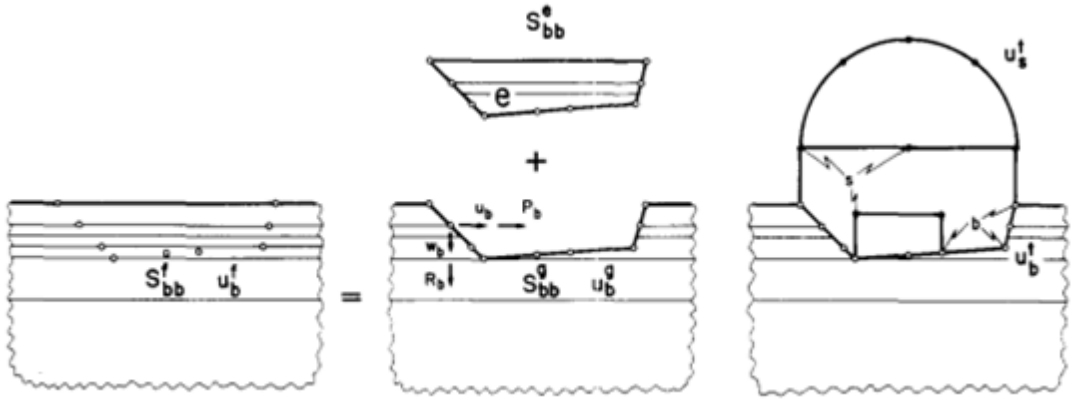

Fig. 2.4. Example depiction of how structures are modeled in soil systems (Wolf, 1987).

Analysis of SSI can be conducted through analytical, numerical, or experimental methods (Jeong et al, 2020; Civelekler et al., 2020; Zhidong et al., 2021; Lou et al., 2011), and to properly predict the SSI and associated properties, engineers use various models consisting of Finite Element Analysis (FEA), Finite Element Modeling (FEM), Discrete Element Modeling (DEM), Finite Difference Modeling (FDM), and Boundary Element Modeling (BEM) (Carbonari et al., 2017; Emani et al., 2009; Kwag et al., 2018; Manna & Baidya, 2010; Abell et al., 2018; Zhao et al., 2017). Analytical methods are considered the simplest to pursue, but its unfortunate drawback is a difficulty in simulating complex loadings and nonlinear force-displacement soil behavior, while numerical methods, specifically FEM, can handle such conditions more appropriately but are computationally more complex to simulate and often require advanced software (Najar et al.,

2025). Tackling a problem utilizing SSI allows for more than one, singular approach to be employed on the path to formulating a solution.

2.4.1 Substructure Method

The term "substructure" has been frequently used thus far without in-depth coverage on its importance. One of the benefits of utilizing SSI is its ability to take a multi-directional approach for modeling interactions between soil and structures. One approach to performing SSI analysis is the use of the substructure method. In this method, the interaction between the soil and structure is partitioned into many interconnected components, known as "substructures", allowing for efficient, flexible computations. (Najar et al., 2025). The substructure method is a simpler method for SSI analysis compared to others, its key strength being its ability to model soil as a force-displacement system. The system can be visualized as discrete system of calibrated springs, which capture the soil medium's response to various forms of loads, excitations, etc. (Wolf, 1987). Fig. 5 depicts the substructure modeled as a system of interconnected springs, known as the "Winkler foundation model" (Bapir et al., 2023).

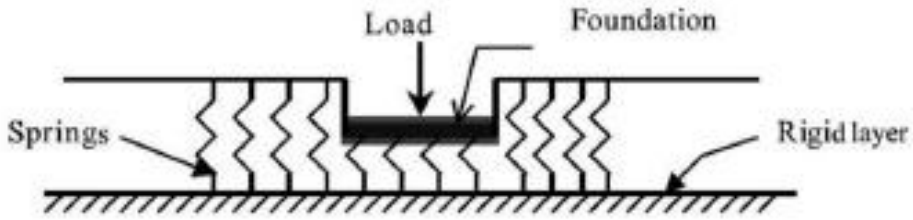

Fig. 2.5. Simple Winkler foundation model (Dutta & Roy, 2002).

Most common interactions are imagined as a structure with a foundation interacting with the surrounding soil (FEMA P-2091). Also known as the "Winkler foundation model," the substructure method makes modeling soil simpler in that soil is represented as a system of independent, interconnected springs instead of a continuous soil medium, where spring stiffnesses

within each "substructure" are calibrated to accurately reflect the modeled soil's natural flexibility and how it realistically resists load, deforms under stress, and displaces (Najar et al., 2025;). While the Winkler foundation model is useful in modeling soil as a linear-elastic medium, it also aids in complex *nonlinear* force-displacement problems which is a more accurate representation in-situ conditions (to be discussed in later sections) (Stewart et al., 2012). These are realized through employing Hooke's Law describing the relationship between load and deflection for any spring (Eq. 2 - 1).

$$F = k \cdot x \qquad (\mathbf{2-1})$$

Where F denotes applied force, k is the coefficient of reaction of the subgrade (spring stiffness) which represents how a soil responds to load, and x gives displacement (Bapir et al., 2023), this equation is a simple representation of the relationship between soil stiffness, load (force), and subsequent displacement from applied load. Kramer (1996) records that each substructure exhibits its own response to loads applied in a discrete manner and are thus estimated separately, the "interconnected" meaning derived by subjecting equal and opposing interaction loads on each node. Najar et al. (2025) notes that SSI and the substructure method have been heavily used in the realm of structural design - buildings approached more staggering heights with advancements in construction capabilities and materials, leading to a necessity of acquiring a more realistic understanding of how staggering static pressures affect the interaction between the infrastructure and underlying soil caused by rigorous static pressures, but since is expanded to account for seismic aspects in design.

Utilization of rings to model soil behavior in soil-structure interaction provides a reasonable approach to basic interactions apparent through elastic soils experiencing loads capable of impermanent deformation. This development, though necessary, is simplistic in modeling soil

media and does not fully consider the plastic deformation processes of soils locally experiencing heavier loads that exceed the medium's elastic zone of deformation. Furthermore, springs alone are imperfect in capturing the true nature of soils where perfectly elastic behavior is not often the case among other properties differing from the ideal. Given this, the present work focuses on developments made in modeling robotic locomotion using concepts and topics relating to cavity expansion theory, transitioning from a simplistic approach of modeling soil using only a mass-spring system to one of more realistic soil action and reaction that still utilizes Hooke's Law for simplicity.

2.5 Cavity Expansion Theory

Methods exist that address problems within SSI and furthermore allow incorporation of substructure method and the Winkler foundation model for applications to solving such problems regarding nonlinear force-displacement soil behavior in subsurface settings. These methods offer insight into the mechanics of how such natural feats in biology and organismal locomotion are conducted, reaction from local soil, energy expenditures, and efficiencies, among others. One method, known as Cavity Expansion Theory (CET), addresses many modeling requirements within geotechnical and subsurface engineering capable of providing such insights. CET is namely concerned with the analysis of changes in stresses, pore pressures, and displacements imparted by expansion and contraction of spherical and cylindrical subsurface cavities; it is a useful method for modeling complex, yet real-world, problems within soil and rock environments (Yu, 2000). It, in its most simple form, allows for analysis of 1D boundary value problems regarding expansion and contraction of cavities.

In the realm of bio-inspired robotics and its role in the development of subsurface infrastructure, accurately estimating stresses and deformations of an expanding subsurface cavity

is a requirement. Utilizing analytical approaches from CET, an analytical framework utilized for its ability to estimate stresses and deformation in an expanding, subsurface cavity, provides such. The method allows for use of a simple SSI spring system presented in this study, can simulate burrow holes of varying geometry, sets zones of deformation around a cavity that accesses elasto-plastic soil behavior and all-while accurately estimates stress and deformation parameters from an expanding cavity (Yu, 2000). By incorporating properties of elastic-plastic soil media, which outlines non-linear force-displacement behavior of an expanding subsurface cavity, work here advances previous developments by utilizing an analytical approach that completes cavity enlargement processes by considering internal normal and tangential forces from previous work of Daltorio et al. (2013) for more accurate results of expansion within the cavity. Originally inspired by natural feats in biology, such as plant root growth and wedging during earthworm locomotion (Ruiz et al., 2015), this study now continues previous work for more efficient robotic locomotion through the subsurface and is useful in other geotechnical engineering applications, such as cone penetration testing, deep foundation analyses, and other applications that consider the usefulness of pressure-expansion relationships (Salgado and Randolph, 2001; Carter et al., 1986).

CET analysis begins with a categorization of two basic types of problems: expansion from a nonzero initial radius and expansion from an initial radius of 0 (Salgado and Randolph, 2001). For this work, focus will be spent on work pertaining to cavity expansion from an initial radius of 0. Consider the 2D profile of a cylindrical cavity under internal pressure imparted by a burrowing earthworm by a series of expansion-contraction steps (Fig. 2.6).

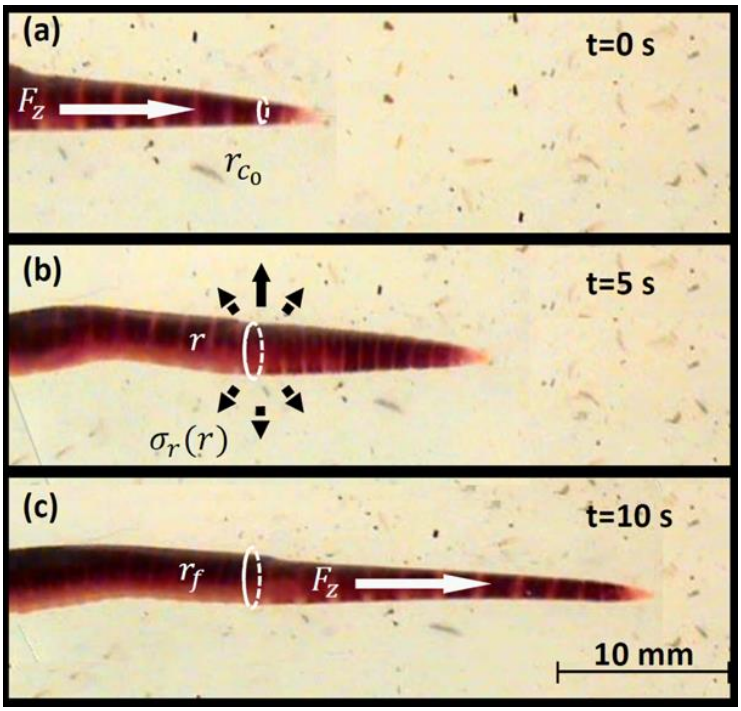

Fig. 2.6. A profile of earthworm's locomotion process illustrated on the internal cavity walls (Ruiz et al., 2015).

The cavity, at equilibrium, is subject to internal radial and circumferential stresses, σ_r and σ_θ, that decays with radius, r, from the center of the cavity to the surrounding soil (Ruiz et al., 2015). In essence, the equation for such phenomenon follows Eq. 2-2 within cavity expansion theory (Ruiz et al., 2015):

$$\frac{\partial \sigma_r}{\partial r} + \frac{\sigma_r - \sigma_\theta}{r} = 0 \qquad (\mathbf{2-2})$$

where such stresses can be visualized in the above figure, r representing radius of the cavity, σ_r denoting radial stress, and σ_θ being circumferential stress. In soils with a weak shear strength parameters and elastic modulus, soil parameters responsible for soil's ability to internally resist (per unit area) failure and sliding along any plane inside it (Das, 2007), the earthworm's locomotion subjects local soil to mechanically transition from between plastic and elastic

deformation, and incorporates Mohr-Coulomb strength criterion that is related to the difference between radial and circumferential stresses all represented in Eq. 3 for such a transition zone (Ruiz et al., 2015):

$$\sigma_r - \sigma_\theta = (\sigma_r + \sigma_\theta)\sin(\phi) + (2s_u)\cos(\phi) \qquad (\mathbf{2-3})$$

where ϕ is the soil's internal angle of friction and s_u is the soil's undrained shear strength, and radial and circumferential stress parameters already defined, the equation relates the transition zone to parameters often dealt with by geotechnical engineers for the elasto-plastic medium of interest. It is necessary to collectively apply these terms to earthworm burrowing because such equations of equilibrium and moving zone of transition depict the process of soil reaction to peristaltic load real-time and provide a mathematical explanation for the act of subsurface burrowing. If analysis of energy expenditure is to be adequately covered in this work, to which is a core focus of this work and in subsequent chapters, it is paramount to discuss the mechanics of subsurface burrowing, which includes local soil reaction. Fig. 2.7 depicts a classic example applied cavity pressure on a thin shell commonly seen in soil mechanics, split zones of plastic and elastic deformation, and a moving elastoplastic boundary, as well as pressure-displacement response recording the phenomenon.

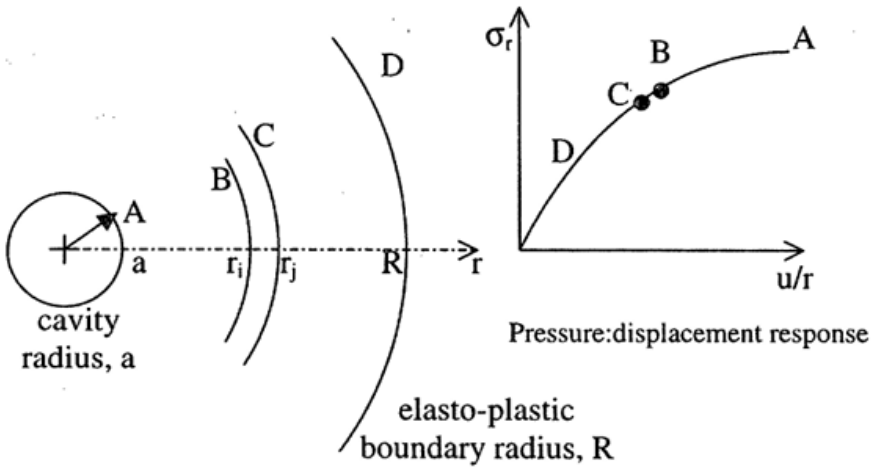

Fig. 2.7: Nomenclature and corresponding pressure-displacement curve (Salgado and Randolph, 2001).

Cavity expansion theory has been applied to analysis in a variety of geotechnical applications and subsurface settings. What started as a method to solve problems related to metal indentation before the of the United States' Industrial Revolution period (Bishop et al., 1945; Hill, 1950), a material quickly concluded to be much simpler than soil media. Moving along further into the 20th century, after stimulation CET received during periods of wartime, it became evident of its importance in understanding wave propagation from subsurface explosions (Salgado and Prezzi, 2007). As years progressed and technology was guided towards a higher level of sophistication, technological advances, specifically those of bio-inspired technology, necessitated incorporation of cavity expansion analysis into design. Afore-mentioned Martinez et al.'s (2019) investigation involved the use of cavity expansion analysis to estimate the dimensions, geometry, and size of an idealized site characterization probe required to initiate self-penetration in sandy, silty, and clayey-simulated soils. Those dimensions were compared to other similar burrowing organisms to evaluate if the results adequately captured the mechanisms of burrowing in soil. Salgado and Prezzi (2007) utilized cavity expansion analysis to base their focus on the CPT

penetrometer's penetration process for cavity creation, deriving a new method for calculation of cone penetration resistance (q_c) in sands. Their work outlined a new, simpler method to obtain cone resistance from cavity limit pressure felt at the cone tip.

Of importance to this work is that of Robert Jaeger's (2012) detailed examination of cone penetration testing in sands, clays, and intermediate soils, best described as coarse and fine-grained mixtures. In such mixtures, effects of drainage condition were on the test were evaluated through numerical modeling simulations as a cylindrical cavity expansion process. Jaeger incorporated a modified form of MIT-S1, a valuable soil constitutive model created by Pestana and Whittle (1999) that is utilized for its ability to simulate multiple soil types, including those of intermediate mixtures, conditions, densities, and stress histories. His work provided an evaluation of a state-normalization of cone penetration resistances in sandy soils with fines. As this work seeks to parametrically extend such studies to model peristaltic movement across a variety of soils and conditions, incorporating the MIT-S1 soil constitutive model into Jaeger's (2018) numerical cavity expansion analysis method provides an adequate means to understanding the process of robot locomotion in many soils expected.

Chapter 3: Methodology

3.1 Background

Previous advancements of Daltorio et al. (2013) within earthworm-inspired robotics focused on modeling the peristaltic locomotion of a segmented, earthworm-like robot within a hollow, rigid media characterized by material that is non-deformable. However, there exists particular inadequacies involving the modeling of soil using rigid media for locomotion through a pre-formed, non-rigid horizontal burrow. Subsequently, a simplified analytical framework was adopted using a sub-structure approach based on soil–structure interaction (SSI) theory to improve the rigid media to one of real-word conditions. The surrounding soil was modeled using a system of independent mass-springs, which is a more appropriate alternative than rigid media in capturing compression, rebound, and deformability properties of real-world soil media. This modeling strategy provided a practical balance between computational efficiency and physical accuracy, enabling detailed analysis of robot–soil interactions without the overhead of fully coupled FEM–DEM simulations that were not fully apparent in analyzing locomotion through rigid media. Furthermore, it served as a valuable tool for validating high-fidelity models and informing the design of adaptive, efficient soft robots for non-destructive underground exploration.

To this end, the robot is modeled using a reduced-order, segment-based structural formulation that is based on the framework by Daltorio et al. (2013). This model is developed in parallel with our Conduit Worm Robot (Mills, 2025) and therefore reflects the same kinematic coupling between axial deformation and radial expansion through a rhombic bar-linkage architecture. In the model, local interaction between each expanding segment and the surrounding soil is modeled through nonlinear radial springs whose force–displacement behavior is derived from cylindrical cavity expansion principles. This form of coupling enables the framework to

capture key soil behaviors, including strain-dependent stiffness degradation, density effects, consolidation history, and drainage conditions, without resorting to full continuum or particle-scale simulations. The resulting dynamic SSI problem is solved iteratively, allowing segment deformation, contact forces, and soil response to evolve consistently throughout locomotion. The framework is applied across sands, silts, and clays under varying density, stress history, and drainages condition to assess how realistic soil behavior governs anchoring capacity, slip, and energetic performance during peristaltic burrowing.

3.2 Robot Model and Soil–Structure Interaction Framework

3.2.1 Physical Platform and Actuation (Peristaltic Conduit Robot)

The earthworm-inspired robot investigated in this study is based on the *Conduit Worm Robot* introduced by Mills et al. (2025) and builds upon the foundational concepts originally proposed by Daltorio et al. (2013). The analytical model follows the same geometric configuration and actuation principles as the physical robot. As shown in Fig. 3-1(a–d), each robot segment consists of a radially repeated two-bar linkage mechanism of rhombic shape in 2D encompassed by an elastomeric skin. This structure enforces a strong geometric coupling between axial length and radial diameter consistent with the constant-volume constraint observed in biological earthworms. From Mills (2025), Fig. 3.1. (a) represents the kinematic design parameters of a single robotic worm segment. Fig. 3.1. (b) depicts an axial view of the segment in the undeformed (top) and actuated (bottom) configurations. Fig. 3.1 (c) represents an exploded view illustrating six radially repeated two-bar linkage assemblies and three servomotors mounted at the posterior end of the segment, and Fig. 3.1 (d) illustrates a schematic of the elastomer skin molding process, in which uncured polyurethane is poured into a 3D-printed mold and allowed to cure around the internal structure (Mills, 2025).

In the unactuated configuration (Fig. 3.1a), the segment has a maximum axial length, x_1, and minimum diameter D_1. Upon actuation, maximum axial compression to position x_2 causes outward expansion of the linkages and an increase in segment diameter to position D_2. The internal linkage skeleton is surrounded by a continuous elastomeric skin (Fig. 3.1d), which provides environmental protection, considerable axial stiffness, and restoring force. As a result, segment deformation under pressure arises from coupled deformation between the internal linkage, the elastomeric skin, and the surrounding medium.

Locomotion is achieved through distributed, segment-level actuation. Each segment incorporates an internal actuator unit that drives controlled axial contraction of the linkage structure. By coordinating the timing and magnitude of actuation across neighboring segments, the robot generates a traveling peristaltic wave along its body, producing alternating phases of anchoring and extension along the body. At any given time, only a small set of segments undergo significant radial expansion and physically engage with the surrounding environment, while adjacent segments experience radial expansion of lower magnitudes and translate axially.

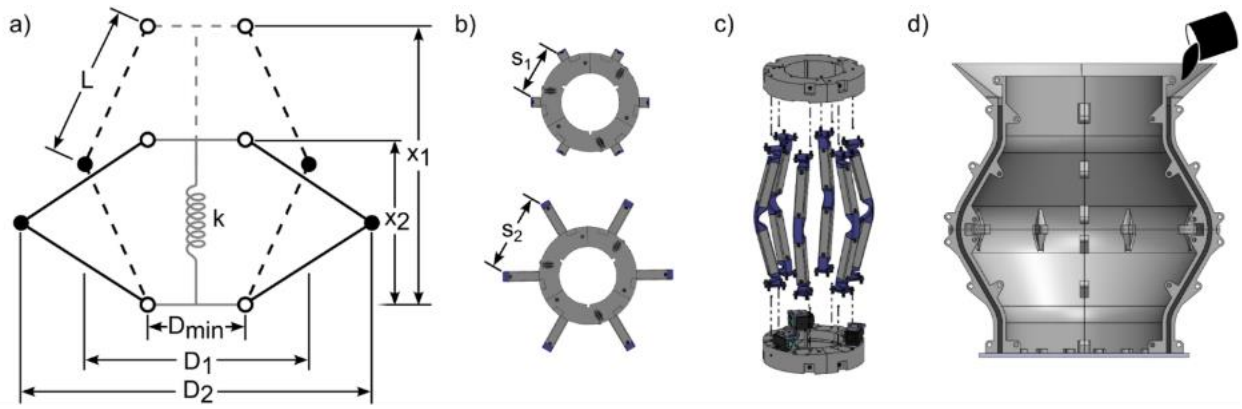

Fig. 3.1. Various illustrations of robot measurements, parts, and components, a) Kinematic design parameters of a single robotic worm segment (Mills, 2025), b) Axial view of the segment (Mills, 2025), c) Exploded view illustrating six radially repeated two-bar linkage assemblies (Mills, 2025), d) Schematic of the elastomer skin molding process (Mills, 2025).

This localized and sequential interaction pattern is significant in the robot's ability to generate propulsion within confined subsurface environments and motivates the segment-level, analytical formulation adopted in this study.

3.2.2 Reduced-Order Segment Model

To enable a tractable analysis of peristaltic locomotion in deformable soil, the multi-segment robot described in Section 3.2.1 is modeled following a reduced-order analytical representation, illustrated in Fig. 3.2. The illustration in Fig. 3.2 does not assume gravitational contact, ground support, or segment drag; instead, the normal and tangential interaction forces that arise from radial segment expansion against the surrounding soil, while neglecting gravitational forces, ground support, and segment drag, this modeling assumption is consistent with the intended operating conditions of conduit-scale robots in horizontal subsurface environments. In Fig. 3.2 (a), segment "*A*" denotes the left-most segment, segment "*i*" is the segment of focus, and segment "*n*" is the right-most and last segment included in the burrowing robot comprised of *n* segments.

Measurements depicted of robot lengths, height, as well as normal and tangential force locations are depicted in Fig. 3.2 (a) and described in subsequent sections.

3.2.2.1 Kinematic Representation and Degrees of Freedom

The robot body is discretized into n deformable segments connected by $n + 1$ axial nodes (Fig. 3.2). Each node possesses a single translational degree of freedom in the axial direction. A radially symmetric, horizontal borehole environment is assumed, and gravitational effects are neglected. Consequently, segments do not rest on or slide along a lower boundary; all contact forces arise exclusively from radial expansion against the surrounding soil as described earlier.

Inspired from Daltorio et al.'s (2013) work on *Softworm*, a generic "*i*" segment is represented as a rhombus-like shape with undeformed axial length l_0 and current resultant axial length, l_i. Due to the rhombus linkage geometry, axial compression induces radial expansion of the segment. The height of segment i, denoted h_i, is defined as the effective radial expansion relative to the undeformed configuration and is kinematically related to segment i length, l_i, through rhombus geometry. For a rhombus linkage with side length l_0, the current segment height is given Eq. 3-1:

$$h_i = \sqrt{l_0^2 - \left(\frac{l_i}{2}\right)^2} \qquad (\mathbf{3-1})$$

here axial contraction directly produces radial expansion.

3.2.2.2 Internal Structural Forces

Elastic resistance to axial deformation is modeled using a nonlinear axial spring acting within each segment. Spring force, $S(l)$, captures the combined stiffness of the linkage skeleton and elastomeric skin and is defined as:

$$S(l) \;=\; K\tan\left(\frac{\pi}{2}\cdot\frac{l_i - l_0}{l_0}\right) \qquad (\mathbf{3-2})$$

where K is a stiffness scaling parameter. Observed experimentally, this form reflects the stiffening behavior of the Peristaltic Conduit segments at large deformations.

3.2.2.3 Actuation Model

The peristaltic mechanism is driven by actuators distributed at each segment. Each segment is subjected to an internal actuator force $F_i(t)$ that induces axial compression, here being segment i at time t. Through geometric coupling, axial compression causes the segment to radially expand. A traveling peristaltic wave is imposed by setting a phase-shifted, sinusoidal actuation pattern. Eq. 3-3 describes a modified actuator force equation originally proposed by Daltorio et al. (2013) as "controller A", this equation represents a sine wave controller that drives the peristaltic pattern:

$$F_i(t) = [\min(A\cdot\sin(2\pi f\cdot t + \phi_i + \phi_{start}) + C, Fmax)]\cdot Ramp(t) \qquad (\mathbf{3-3})$$

Where A is the force amplitude, f is the actuation frequency, f_i is the spatial phase shift for segment i, f_{start} is an optional initial phase offset, C is a constant and $F_{\max}$ enforces an upper limit on actuator force. Daltorio et al. (2013) also included a parameter to enforce gradual increase of actuator force amplitude in the actuator force equation. The R_{amp} function, given in Eq. 3-4 at time t,

$$R_{amp}(t) \;=\; \min\left(\frac{t}{t_{Ramp}},\, 1\right) \qquad (\mathbf{3-4})$$

gradually increases actuation during startup (until the considered wave period (t_{Ramp}) to avoid transient slip. As proposed by Daltorio et al. (2013)'s work on *Softworm* and based on the work of Boxerbaum et al. (2012), this robot possesses a rotating cam mechanism with cables attached to segments and pulled in sequence. Segments are extended at any given time based on evenly spaced rotations of the cam. This allows an individual segment to undergo a continuous cycle of all

possible rotation actuations within the full period of the cam rotation Each discrete segment is prescribed the same waveform shifted by a fixed time, which is accomplished by knowing each individual location of cable origins about the circumference of *Softworm* relative to other actuators along the body, enabling the traveling wave. The actuator force of the simulated robot includes this parameter to accurately model the same phase shift of peristaltic waves. The spatial phase shift is based on the work of Boxerbaum et al. (2012), defined as:

$$\phi_i = \alpha \cdot (i - 1) \cdot l_0 \qquad (\mathbf{3-5})$$

where *a* is selected from one full sine wave, a desired number of waves down the length of the body, and the length of the robot based on the number of body segments combined to produce a smooth traveling wave along the body, and *i* denotes segment *i*. A backward-traveling peristaltic wave is assumed, which has been shown to produce forward motion (Dorgan, 2018)

3.2.2.4 Contact Forces with the Surrounding Boundary

Contact between the robot and the surrounding soil is assumed to be local. At any time during robot movement, only a portion of total segments are actively engaged with the boundary through radial expansion, while neighboring segments primarily translate energy axially with minimal radial deformation. This observation motivates a segment-level representation of soil–robot interaction, in which contact forces are applied only at segment that expand sufficiently to physically engage with the surrounding soil. Contact is assumed to occur when the tip of the radially expanded segment exceeds the borehole radius, at which point radial deformation of the surrounding soil occurs. Upon such contact, the interaction forces acting on the i^{th} segment are decomposed into two components representing reaction forces:

1. Normal forces (N_i), which act radially inward and resist further expansion. These forces govern anchoring capacity and are determined by the mechanical response of the surrounding soil or confining boundary.
2. Tangential forces (T_i), which act along the axial direction and arise through Coulomb friction at the contact interface. Tangential forces are modeled using Coulomb friction, $T_i = \mu * N_i$, where μ is the kinetic friction coefficient. These forces resist relative axial slip between the robot and the surrounding medium and are responsible for thrust generation, thereby denoting these forces acting opposite of the "forward" direction of motion.

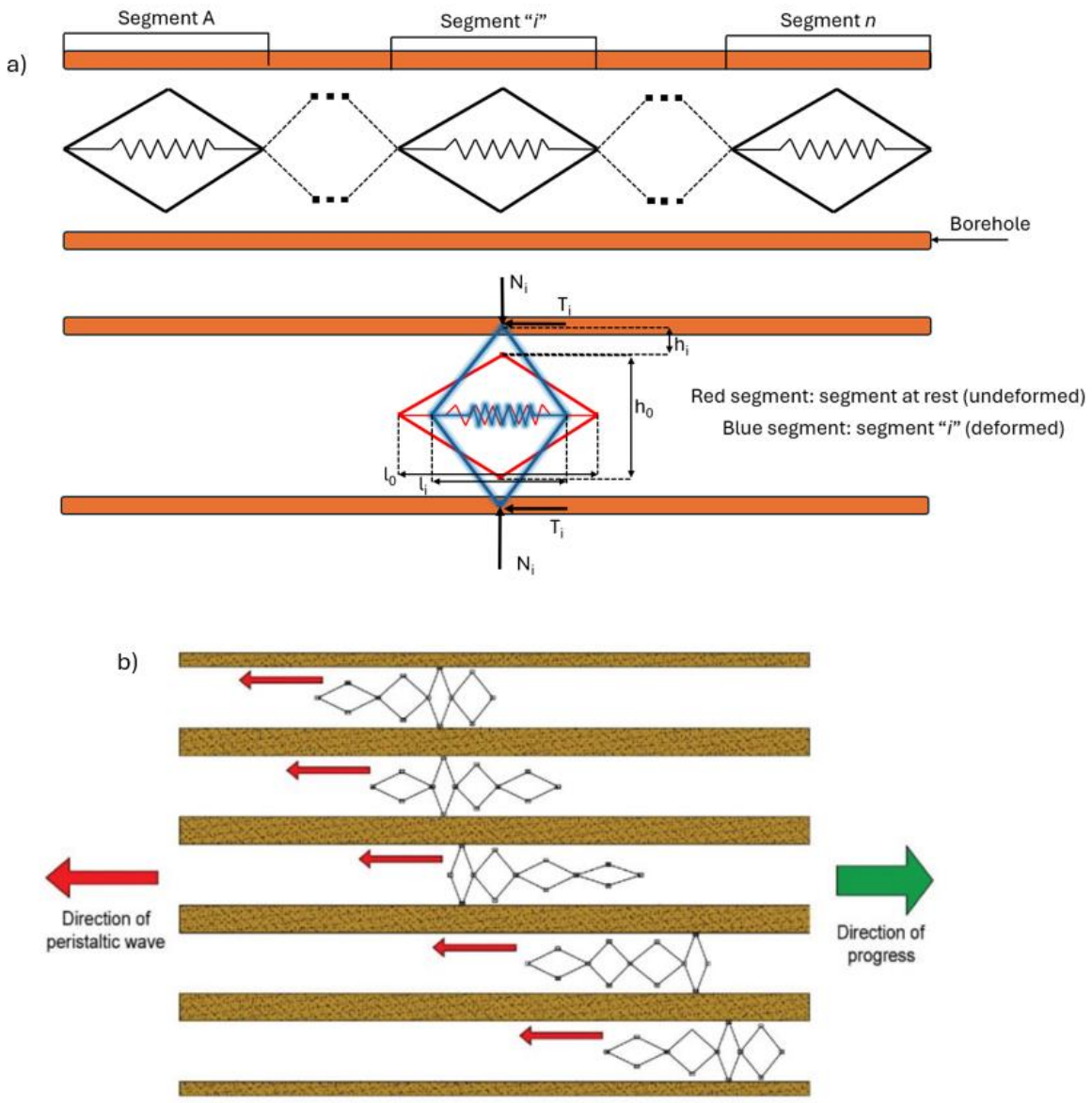

Fig. 3.2. a) Schematic representation of a multi-segment earthworm inspired robot model, complete with measurements pertaining to a deformed and undeformed segment. b) Peristaltic locomotion of an earthworm robot with 4 segments inside of a borehole.

3.2.2.5 Governing Equations of Motion

Applying d'Alembert's principle and following the formulation of Daltorio et al. (2013), the equation of motion for node *i* can be written as:

$$ma_i - S(l_i) + S(l_{i-1}) + k\left[-\frac{\theta_{i-1}}{h_i} + \frac{\theta_i}{h_{i+1}} + \frac{\theta_i}{h_i} - \frac{\theta_{i+1}}{h_{i+1}}\right]\ldots$$

$$-[T_i + T_{i+1}] - [N_i + F_i]\frac{l_i}{h_i} + [N_{i+1} + F_{i+1}]\frac{l_{i+1}}{h_{i+1}} = 0 \qquad (\mathbf{3-6})$$

where m is the nodal mass, a represents position along the x-axis (contact point location), l_{i-1} is resultant segment length at segment i - 1, k is the inter-segment torsion spring stiffness, θ_{i-1}, θ_i, and θ_{i+1} denotes torsion spring angle between links at segment i - 1 , segment i, and segment i + 1, respectively. This equation highlights how internal elastic forces, actuation, and contact forces jointly govern segment dynamics.

3.2.2.6 Energetic Metrics

Frictional energy dissipation during locomotion, proposed by Daltorio et al. (2013) is quantified by the cumulative slip work, L^t:

$$L^t = -\sum_{i=1}^{n}\int_{Path}^{2} T_i^t \; d_{x_i}^{-t} \approx \sum_{i=1}^{n}\sum_{\tau=\Delta t}^{t}\left[T_i^{\tau} + T_i^{\tau-\Delta t}\right] \cdot \left[x_i^{\tau-\Delta ti} - x_i^{\tau} + x^{\tau}{}_{i-1}^{-\Delta t} - x_{i-1}^{\tau}\right]/2 \;\; (\mathbf{3-7})$$

where n is number of segments, x is segment location, τ is time period (seconds), and $\bar{x}_i^t$ is midpoint location of segment i at time t. The frictional Cost of Transport (COT) with respect to the total robot mass $M = m(n+1)$, where node mass is represented by m and number of segments by n, is the frictional energy loss per unit distance travelled, normalized by mass. Using the cumulative slip work L^t defined in Eq. (3-7) originally proposed by Daltorio et al. (2013). The instantaneous cost of transport (frictional COT) can be defined using Eq. (3-8).

$$COT = \frac{1}{M} \cdot \frac{dL^t}{dx} \qquad (\mathbf{3-8})$$

Where L^t is defined in Eq. 3-7, and x representing the center-of-mass displacement. To provide an upper bound on energetic demand, a worst-case frictional cost of transport is also defined by assuming continuous sliding at all contacts,

$$COT^f_{worst} = \frac{2\mu sliding}{M} \sum_{t=t_f-\tau}^{t_f} \sum_{i=1}^{n} N_i^t \frac{\Delta t}{\tau} \qquad (\mathbf{3-9})$$

where $\mu_{sliding}$ is the kinetic friction coefficient, N_i^t is the normal force at contact i at time t, and Δt is the simulation time step. This metric isolates the energetic impact of normal force magnitudes independent of instantaneous slip dynamics.

This reduced-order representation preserves three essential features of the physical robot: (1) geometric coupling between axial compression and radial expansion is maintained through the rhombus kinematics; (2) elastic (potential) energy storage and release is captured through internal segment springs; and (3) localized soil interaction is modeled at the segment-level, consistent with the physical observation that anchoring occurs segment-by-segment discretely rather than continuously along the body.

3.2.3 Soil Compliance Representation via Cavity Expansion Theory

To represent the mechanical response of the surrounding soil while retaining computational efficiency, soil–structure interaction is modeled using discrete nonlinear radial springs whose force–displacement relationships are derived from cylindrical cavity expansion theory (CET). This approach represents the borehole wall deformed locally caused by radial expansion of robot segments, capturing strain-dependent stiffness degradation, yielding, and stress-history effects without resorting to full continuum or particle-scale simulations.

3.3 Cavity Expansion Theory

3.3.1 MIT-S1 Soil Constitutive Model

The soil constitutive model is quite an important topic incorporated in this work. Soil constitutive models are mathematical representations of the stress-strain behavior of a specific soil under load, relating stresses applied to strains experienced as an effect of such stresses (Briaud, 2023). In simple terms, a soil constitutive model can be depicted through Hooke's Law (refer to Eq. 2 – 1), where stiffness of soil at a location of applied load yields a linear force-displacement relationship, and the parameters within the relationship are quite easy to predict. The formulation and evaluation of more complex effective stress constitutive models, such as those with capabilities of predicting nonlinear force-displacement relationships and can reliably simulate the complex stress-strain-strength characteristics of a soil of interest, is an iterative process that extends predictive capabilities through control of clearly defined input parameters (Pestana and Whittle, 1999). The importance of such models stems from the need of any geotechnical engineering work – the desire to understand the short- and long-term effects of soil disturbance under effects of stresses on soil. When excavations and underground work, tunnelling projects, for example, are carried out in dense, urban environments, the importance to accurately predict deformations in the subsurface is necessary to preserve existing infrastructure and ensure safety at all levels. In such deep excavation projects, such as retaining systems, soil-structure interaction is affected by a multitude of complex factors – soil response being the foremost, detailing nonlinear stress-strain response, anisotropy, and rate effects common in natural, real-world soils (Kullingsjo, 2009).

Researchers at MIT (Massachusetts Institute of Technology) formulated a series of generalized effective stress constitutive models for cohesive soils, one of which being MIT-E3 soil

constitutive model. MIT-S1, presented by Pestana (1994), follows after its predecessor, MIT-E3, developed by Whittle (1987), both elasto-plastic soil constitutive models. This was done by advanced laboratory testing to evaluate and determine various soil parameters needed to most accurately simulate soil behaviors (see Table 3-1). MIT-S1 soil constitutive model expands the capabilities of MIT-E3 to include non-cohesive and intermediate soils, such as sands, silts, and mixtures with more cohesive-like soils. Once more, MIT-S1 allows for manipulation of density states, stress histories, as well as drainage conditions, of deposited soils, through reportedly a reduced amount of model input parameters required for simulation under different loading conditions (Kullingsjo, 2009). This significantly increased the depth of analyses that could be performed for geotechnical applications, including enabling the work presented in later sections of this report.

3.3.2 Cavity Expansion Framework

Cavity expansion theory (CET) idealizes the soil as a continuum surrounding an expanding cylindrical cavity and provides a rigorous framework for predicting the relationship between radial pressure and cavity deformation during localized intrusion (Vesic, 1972; Yu and Houlsby, 1991; Salgado and Randolph, 2001; Chen and Abousleiman, 2018). By solving the coupled stress–strain fields around the cavity, CET captures elastic–plastic deformation, stiffness degradation, and the evolution of confining pressure during expansion. These features make CET well suited for modeling the radial expansion of peristaltic robot segments against surrounding soil. Fig. 3.3 depicts the elastic and plastic regions of a subsurface cavity subjected to load.

According to Salgado and Prezzi (2007), after a cavity is created, a plastic zone is created in local proximity of the cavity with a radius, R. Immediately bound to its exterior is the nonlinear elastic zone with radius, A. Beyond this zone is a linear elastic zone. In the linear elastic zone,

shear strains are smaller than threshold strains allowing the soil in this region to continue to behave elastically (soil stiffness can be modeled as a linear force-displacement curve). In the nonlinear elastic zone, stresses have not reached peak failure, but shear strains are larger than the elastic zone threshold strain. Behavior is nonlinear elastic, so the force-displacement relationship changes (although linearly) with each iteration. Linearity follows Hooke's Law. Finally, the plastic zone of deformation contains nonlinearity. This zone is classified as one where limit pressure, or peak pressure required to radially expand the cavity. The material in this region has failed and is expanding radially with each timestep, permanently deforming.

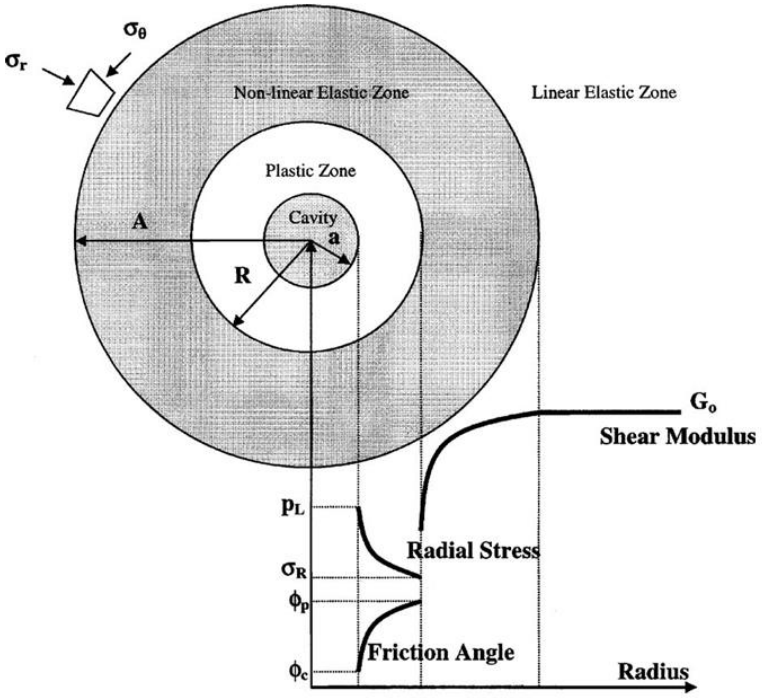

Fig. 3.3. Elastic and plastic zones of deformation of an expanding subsurface cavity (Salgado and Prezzi, 2007).

In this study, cavity expansion analyses were performed using the ASCEND (Applications for Spherical and Cylindrical Cavity Expansion in Nonlinearly Deforming Geomaterials) code developed by Jaeger (2018). ASCEND is based on the semi-analytical formulations for drained

and undrained cylindrical cavity expansion proposed by Chen and Abousleiman (2012, 2013). While these original formulations employed Cam Clay and Modified Cam Clay constitutive models, ASCEND extends the framework by incorporating the MIT-S1 constitutive model (Pestana and Whittle, 1999). This enhancement enables accurate simulation of a wide range of geomaterials, including sands, silts, clays, and mixed soils across different density, consolidation, and drainage conditions (Jaeger, 2012; Price, 2018). A key advantage of ASCEND is its ability to account for initial stress anisotropy, which is common in both natural and engineered ground conditions. This capability allows cavity expansion behavior to be evaluated under isotropic and anisotropic in-situ stress states, improving the accuracy of soil stiffness relationships. The validity and robustness of ASCEND for modeling nonlinear soil response have been demonstrated in numerous prior studies, including applications to subsurface intrusion and soil–robot interaction problems (Martinez et al., 2020; Chen et al., 2022; Chen et al., 2024). In the present work, the pressure–displacement relationships obtained from ASCEND are used directly to define the nonlinear spring behavior governing soil resistance to segmental expansion in the peristaltic locomotion model.

For a cylindrical cavity of initial radius a_0, ASCEND computes the relationship between cavity pressure p and radial expansion Δa, accounting for elastic and plastic deformation of the surrounding soil (Eq. 10). The resulting pressure–displacement curve is used directly to define the nonlinear stiffness governing soil resistance to segmental expansion.

$$p = p \cdot \Delta a \qquad (\mathbf{3-10})$$

3.3.3 Mapping CET Response to Segment-Level Springs

Within the reduced-order robot model, each segment that contacts the surrounding soil is assigned an independent radial spring acting normally to the borehole wall. The normal force acting on the i^{th} segment is expressed as

$$N_i = p_i \cdot A_i \qquad (\mathbf{3-11})$$

where p_i is the cavity pressure corresponding to the local radial deformation and A_i is the effective contact area of the segment. In this study, A_i is taken as the circumferential contact area of the expanded segment over its effective axial contact length, i.e.,

$$A_i = 2 \cdot \pi \cdot a_0 \cdot L_c \qquad (\mathbf{3-12})$$

where a_0 is the initial borehole radius and L_c is the axial contact length of a segment, assumed constant. The tangent stiffness of the soil spring is obtained from the cavity expansion response as:

$$k_{s,i} = \frac{dp}{d(\Delta a)} A_i \qquad (\mathbf{3-13})$$

allowing the resistance to evolve nonlinearly with increasing deformation. This formulation naturally captures degrading stiffness, yielding, and stress relaxation during expansion.

According to CET, soil deformation is assumed to be localized. During each soil–structure interaction update, only the active segments in contact with soil induces radial deformation of the surrounding soil. Adjacent segments influence global equilibrium through internal structural coupling but do not induce additional local soil deformation during that iteration. This is applicable to other peristaltic waveforms, such as those that deform the geometry of multiple segments into contacting the conduit in which they encapsulate at the same instance.

3.3.4 Selected Soil Types and Conditions

To span a broad range of geotechnical conditions relevant to subsurface infrastructure, three representative soils were selected: (1) Toyoura sand, representing clean to silty sands with stress-dependent stiffness and dilative behavior; (2) Non-plastic silt (silica flour), representing intermediate permeability fine-grained soils; (3) Boston Blue Clay, representing structured clays with strong sensitivity to consolidation state and drainage. The calibrated MIT-S1 constitutive parameters for each soil are summarized in Table 3-1, developed by Pestana and Whittle (1999).

Table 3-1: MIT-S1 calibrated soil parameters

Parameter	Description	Toyoura sand	Silt (Silica flour)	Boston blue clay
ρ_c	Compressibility of sand in the limiting compression curve regime and virgin compressibility line of clays.	0.37	0.33	0.178
p'_{ref}/P_{atm}	reference stress normalized by atmospheric pressure at void ratio = 1.	55	60	1.5
θ	Transition compression behavior.	0.2	0.6	0
D	non-linear volumetric swelling.	0	0	0.04
r	volumetric hysteresis response.	0	0	0.3
h	Irrecoverable plastic strain of the unload-reload cycle.	2	2	6
K_{0NC}	The lateral pressure ratio in the limiting compression curve regime.	0.49	0.49	0.49
C_b	Small strain elastic compressibility.	750	899	540
μ'_0	Poisson's ratio at load reversal.	0.14	0.23	0.24
ω	Non-linearity in Poisson's ratio.	1	1	1
ω_s	Small strain non-linearity in shear.	2.5	4	8
φ'_{cs} (°)	Critical state friction angle.	31	33	33.5
φ'_{mr} (°)	Apex angle of bounding surface.	28.5	11.5	46
P_φ	Transition from contractive to dilative soil behavior.	2.45	3.3	0
m	Shape of bounding surface.	0.55	0.45	0.8
ψ_p (°)	Rate of evolution of anisotropy due to stress history.	50	50	8

For each material, multiple mechanical states were considered to capture realistic variability:

- For the sandy soil, three packing states were evaluated using the state parameter ξ, ranging from dense (ξ= -0.1) to loose (ξ= 0.1).
- For the non-plastic silt, dense (ξ= -0.1) and medium-dense (ξ= 0) states under drained and undrained conditions were considered.
- For the clayey soil, four over-consolidation ratios (OCRs), spanning normally consolidated to heavily over-consolidated conditions.

Together, this selection spans a broad spectrum of soil behaviors when interpreted in the context of the Robertson (1990) Soil Behavior Type (SBT) chart, as illustrated in Fig. 3.4. Specifically, the chosen materials and mechanical states cover zones ranging from clean sands and sand mixtures to silts and stiff fine-grained soils, encompassing wide variations in density, frictional resistance, compressibility, stress history, and sensitivity. Green markers indicate the selected states. Clayey soils are represented by four over-consolidation ratios (OCRs), sandy soils by three packing states defined using the state parameter ξ, and non-plastic silts by two packing states. Together, these selections span clean sands, sand mixtures, silts, and stiff fine-grained soils, covering a broad range of density, stiffness, and stress-history conditions. This diversity ensures that the analytical framework captures not only contrasts between soil classes, but also the influence of density, consolidation history, and drainage behavior on stiffness degradation, evolution of cavity pressure, and energy dissipation during peristaltic locomotion. As a result, the proposed soil–structure interaction model is applicable across a wide range of geotechnical conditions.

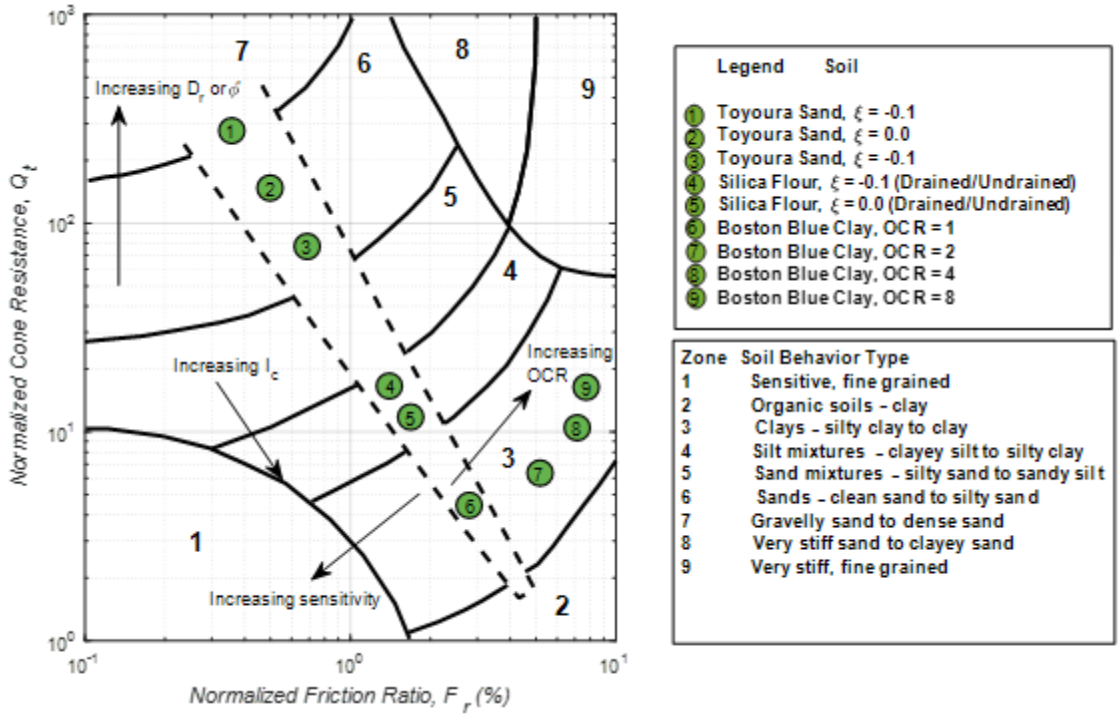

Fig. 3.4. Soil types and mechanical states considered in this study plotted on the Robertson (1990) normalized Soil Behavior Type (SBT) chart.

3.3.5 Local Consistency Condition Between Segment Deformation and Normal Force

Because soil compliance and segment deformation are interdependent, the normal contact force cannot be prescribed a priori. Instead, a local consistency condition must be enforced between segment expansion and soil reaction. To clarify this coupling, a small-perturbation analysis is performed for a contacting segment i. A differential increase in segment height, δh_i, is imposed while the segment remains in contact with the surrounding soil. Consistent with the localized anchoring observed in the physical robot, adjacent segments i - 1 and i + 1 are assumed to undergo rigid-body motion only and therefore do not experience changes in deformation during this perturbation (Fig 3.5).

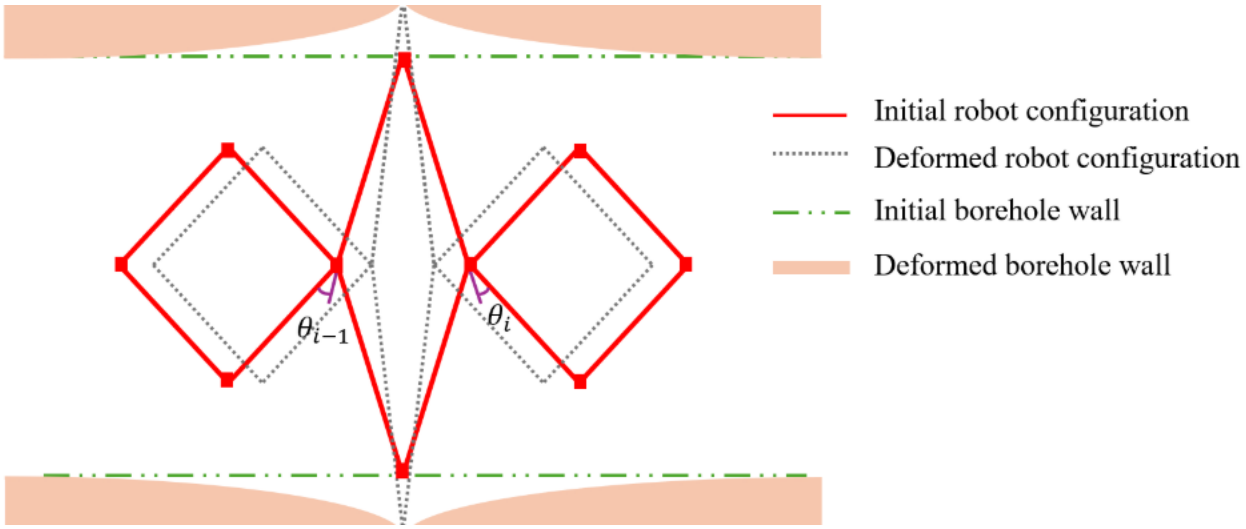

Fig. 3.5. Schematic view of the initial and deformed situation of the contacted segment (with borehole wall) and its influenced neighbors.

Neglecting inertial and actuation forces, the local force balance at segment i reduces to a quasi-static equilibrium relation between the segment's internal force, dependent on height h_i and the normal contact force N_i. Linearization of this equilibrium yields the first-order relationship:

$$\delta N_i \approx -K_i(h_i, N_i) \cdot \delta h_i \qquad (\mathbf{3-14})$$

where K_i is a positive-valued function that incorporates internal segment stiffness, inter-segment torsional resistance, frictional interaction, and soil compliance.

The negative sign indicates that an increase in segment height (radial expansion) leads to a reduction in reaction normal force under deformable confinement. Physically, this reflects the redistribution of actuator work into soil deformation rather than rigid reaction since normal force is being reduced (in which case, it does not in rigid media). Numerically, Eq. (14) provides the update rule used within the soil–structure interaction iteration to revise the normal force estimate for a given trial segment deformation.

3.4 Coupled Soil–Structure Interaction Solution, Numerical Workflow, and Performance Metrics

The soil–structure interaction formulation developed previously establishes an implicit coupling between segment deformation and normal contact force from applied load onto under deformable confinement. When a segment expands against the surrounding soil, the resulting normal force delivered from soil reaction depends on the amount of soil deformation, while the soil deformation itself depends on the magnitude of the applied normal force. As a result, neither the segment height nor the normal reaction force can be prescribed *a priori,* and both must be determined simultaneously in a self-consistent manner. At each iteration, Eq. (3-14) provides the local update linking incremental segment deformation to the corresponding reduction in normal force.

The dynamic simulation is implemented in a custom MATLAB framework and advanced in discrete time steps. At the beginning of each time step, the equations of motion are first solved assuming a rigid confining boundary. This step is equivalent to classical pipe-confined peristaltic robot models and yields a reference normal force corresponding to zero wall deformation. The rigid-boundary solution serves three purposes: it provides an initial estimate for contact forces, establishes an upper bound on admissible normal reaction, and defines a baseline against which the influence of soil compliance can be quantified. Plainly stated, data from the equations of motion are solved assuming a rigid soil media which assigns a baseline maximum for reaction normal force exerted on the segment as it radially expands into the medium – reaction normal force in deformable soil media can only be less than or equal to the magnitude of this value in a discrete manner where timesteps are of importance as well.

When a segment expands sufficiently to contact the borehole wall or surrounding soil, the rigid-boundary assumption is then relaxed and replaced by a compliant boundary made up of nonlinear radial springs derived from cavity expansion theory. For each segment in contact with the boundary (borehole wall), an iterative soil–structure interaction correction is performed. In this procedure, the current estimate of normal force is used to compute local soil deformation from the cavity-expansion-derived pressure–displacement relationship. The resulting soil deformation modifies the segment height, which in turn updates the normal force through the local force–deformation sensitivity relation. The updated normal force is required to satisfy two physical constraints: it must be less the rigid-wall reaction force, and it must correspond to nonzero soil deformation, reflecting the compliant nature of the surrounding ground. A soil deformation equal to zero reflects a rigid boundary condition in which case reaction normal force is at its peak magnitude. For deformable soil media, reaction normal force must always be less than this peak value in magnitude.

To maintain computational efficiency and consistency with the physical anchoring mechanism of peristaltic locomotion, soil deformation is assumed to be localized. During each iteration, only segments actively in contact with the boundary undergo radial deformation, while adjacent segments are treated as rigid bodies and experience only rigid-body translation. After each update of contact forces, global equilibrium of the robot is enforced by re-solving the equations of motion. This iterative procedure continues until convergence is achieved between the predicted segment deformation and the corresponding normal force based upon a pre-defined tolerance value. Once convergence is reached, the robot configuration is advanced to the next time step and the process is repeated. The overall numerical workflow is summarized in Fig. 3.6.

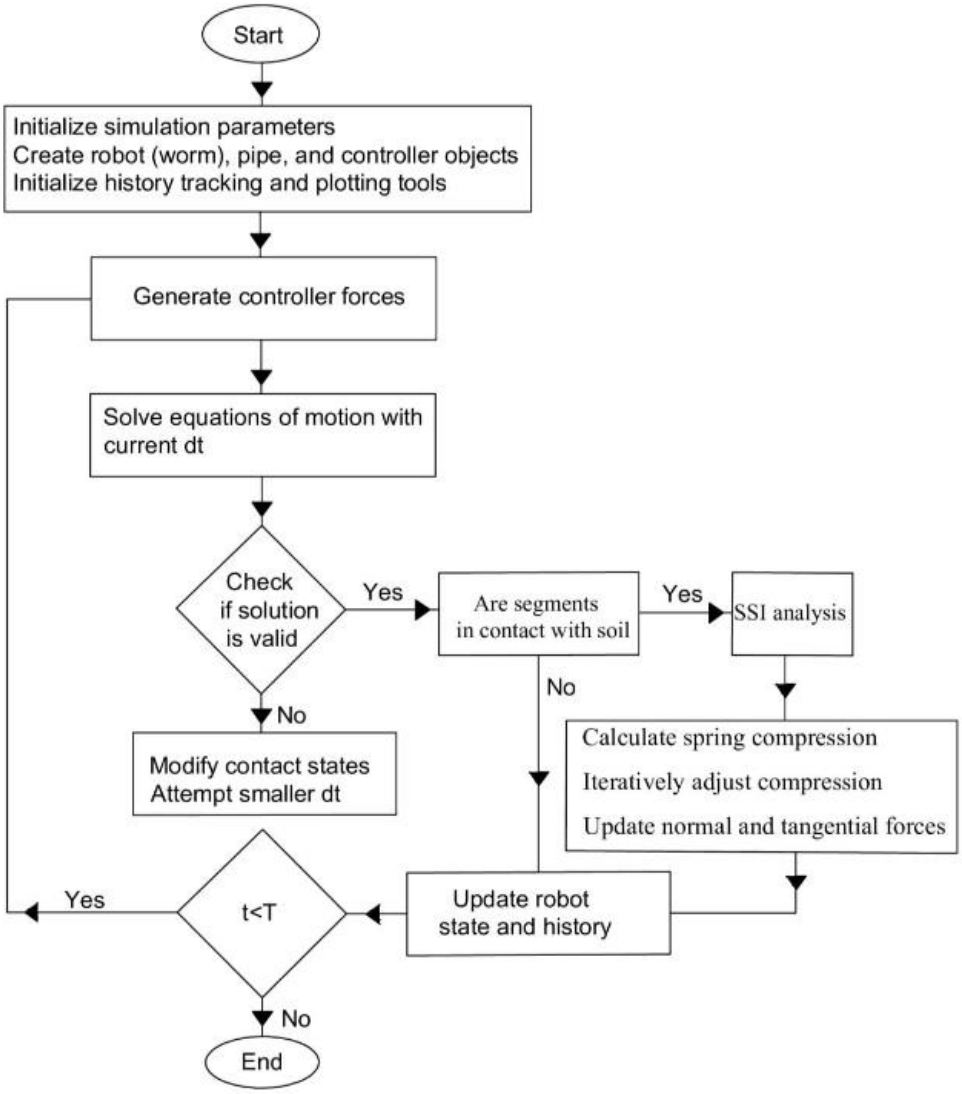

Fig. 3.6. Logic flowchart of the peristaltic locomotion simulation in deformable soil within the analytical framework

Chapter 4: Results and Discussion

4.1 Introduction

The analytical and numerical framework developed in Chapter 3 enables a systematic evaluation of how deformability properties of soil, nonlinear relationships in stiffness, density, consolidation history, and drainage conditions influence peristaltic locomotion in earthworm-inspired robots. Central to such locomotion is the development and characterization of segment-level contact forces, which govern anchoring, slip, and energy dissipation during expansion–extension cycles.

Fig. 4.1 illustrates the robot geometry in unactuated (relaxed) and actuated (in-motion) configurations within an example horizontal borehole. As depicted, when actuator forces are applied, individual segments undergo axial compression and radial expansion until segment contact is established with the surrounding soil. Once sufficient anchorage is achieved, made possible through contact forces, axial extension of adjacent segments produces forward motion. At any given time, multiple contact states may coexist along the body, including sticking contact, pure normal contact, and left or right slip, while non-contacting segments translate freely according to the actuation waveform. The resulting forward progression of the robot center of mass (COM), together with the evolving contact states of individual segments, is shown in Fig. 4.2. Fig. 4.2 (a) shows the initial static configuration of the worm body segments within the confined environment; while Fig. 4.2 (b) depicts peristaltic locomotion phase where the robot executes segment expansion and contraction to generate forward thrust; and lastly, Fig. 4.2 (c) Spatiotemporal history trace illustrating the contact state distribution over time during a certain part of locomotion (The horizontal axis represents the position in the hole, the vertical axis denotes the virtual time sequence).

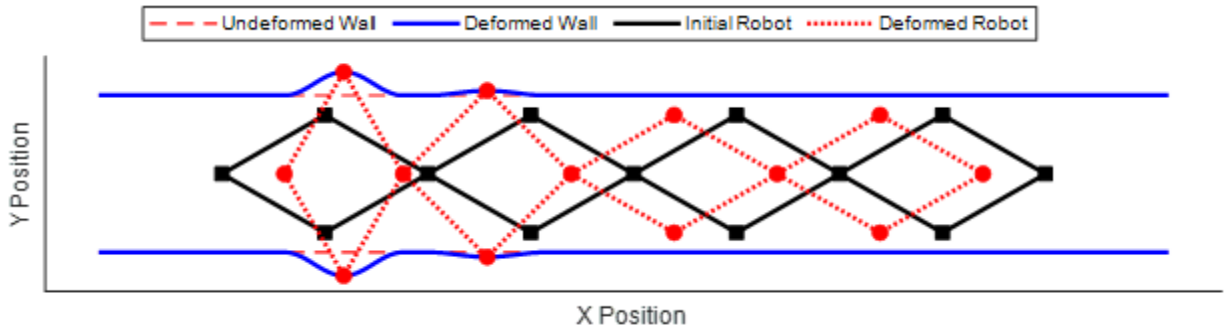

Fig. 4.1. Robot geometry seeking enough anchorage to proceed with its locomotion inside the borehole.

As stated, previous analytical models of peristaltic locomotion, such as those proposed by Daltorio et al. (2013), assumed rigid borehole walls. Replacing a deformable boundary with a rigid one leads to overestimation of interaction forces, particularly the normal forces (which directly control frictional resistance through $T=\mu*N$). In simpler terms, the contact forces present during radial expansion are larger than required for borehole expansion. When the surrounding boundary is deformable, a portion of actuator work is spent deforming the soil rather than being transmitted back to the robot as reaction force. This effect fundamentally alters anchoring and must be accounted for to obtain physically realistic predictions.

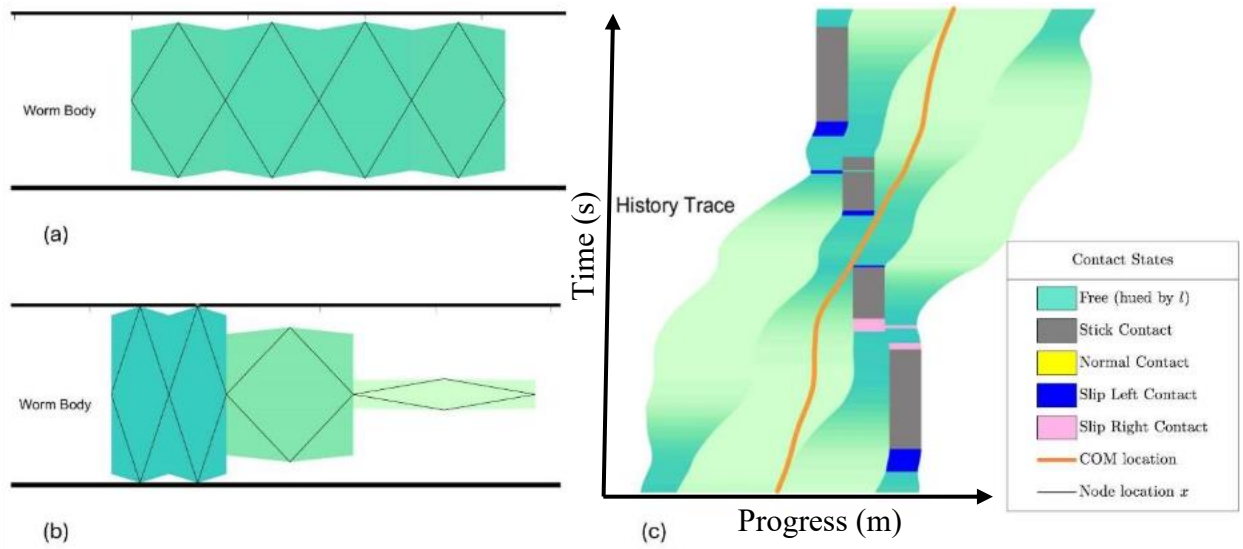

Fig. 4.2. Overview of robot configuration and locomotion history: a) Initial static configuration of the worm body segments, b) Peristaltic locomotion phase, c) Spatiotemporal history trace.

To quantify the impact of wall compliance on normal force, the Normal Force Ratio (NFR) is introduced in Eq. 4-1 as:

$$NFR = 1 - \frac{N_m}{N_r} \qquad (\mathbf{4-1})$$

where N_r is the normal force under the rigid wall (baseline) condition and N_m is the modified normal force accounting for soil–structure interaction effects. The NFR provides a normalized measure of the reduction in normal force resulting from wall deformability. In the extended simulation framework, normal forces are updated by accounting for spring compression present at borehole walls that represent local wall deformation at contact points. When a segment contacts such a boundary, the surrounding soil deforms in response to the applied load, reducing the magnitude of reaction force transmitted back to the robot. The amount of wall deformation is computed iteratively and used to update the segment height and force distribution along the robot

body. Notably, in the non-contact scenario, or if soil–structure interaction is ignored, $N_m = 0$, and when wall compliance is considered, the contact force reduces due to the energy absorbed by wall deformation, leading to $0 < N_m < N_r$, and hence $0 < NFR < 1$.

To ensure consistent interpretation across all parametric studies, robot performance and soil–structure interaction are evaluated using four complementary metrics that together capture force transmission, anchoring effectiveness, locomotion efficiency, and energetic cost. Specifically, results are analyzed in terms of (i) the Normal Force Ratio, which quantifies the reduction in normal contact force relative to a rigid-wall baseline and serves as a direct measure of boundary compliance effects, (ii) the maximum normal force, N_{max}, which reflects the peak anchoring capacity developed instantaneously by the robot during each actuation cycle, (iii) the center-of-mass position over time, which provides a direct measure of net forward progression and slip accumulation, and (iv) the cost of transport, derived from cumulative frictional work and normalized by travel distance and robot mass, which quantifies locomotion efficiency. The parametric testing plan used in this study is summarized in Table 4-1.

Table 4-1. The parametric testing plan used in this study, constructed to isolate the influence of soil density, drainage condition, and preloading history on anchoring behavior across granular, transitional, and cohesive soils.

Soil class	Relative density / state	OCR	Drainage condition	Robot stiffness	Purpose in simulation plane
Sand	Loose	—	Drained	K	Represents low-stiffness granular behavior and lower anchoring capacity
Sand	Medium dense	—	Drained	K	Represents intermediate granular stiffness and anchoring response
Sand	Dense	—	Drained	K	Represents high-stiffness, dilative granular behavior and strong anchoring
Silt	Medium dense	—	Drained	K	Represents transitional soil behavior between sands and clays
Silt	Dense	—	Drained	K	Represents higher-stiffness, drainage-sensitive transitional behavior
Clay	NC	1	Undrained	K	Represents soft cohesive soil with low effective stiffness
Clay	OC	2	Undrained/ Drained	K	Represents moderate preloading and increased stiffness
Clay	OC	4	Undrained/ Drained	K	Represents significant stress history and reduced NFR
Clay	OC	8	Undrained/ Drained	K	Represents highly preloaded, stiff cohesive behavior
Sand	Medium dense	—	Drained	0.5K	Represents effects of the robot stiffness on the behavior
Sand	Medium dense	—	Drained	1.5K	Represents effects of the robot stiffness on the behavior
Sand	Medium dense	—	Drained	2K	Represents effects of the robot stiffness on the behavior

4.2 Role of Soil Compliance on Anchoring and Locomotion

We first establish a rigid borehole as a baseline case to isolate the role of soil deformability in peristaltic locomotion. This reference condition corresponds to the classical assumption adopted in many prior studies, in which the confining boundary cannot deform under load and all radial segment expansion is resisted kinematically by the borehole wall. The results under linear and nonlinear soil models are then interpreted relative to this baseline to quantify how increasing levels of compliance and stiffness nonlinearity alter force transmission, anchoring behavior, and locomotion performance.

Under rigid borehole conditions, the confining boundary is assumed not compliant, such that all radial expansion imposed by the robot must be resisted by normal reaction forces. As shown in Fig. 4.3(a), which reflects NFR within various simulations, the NFR remains zero throughout the entire locomotion sequence for rigid media, while in both linear and nonlinear media (which refers to the relationship between force and displacement within Hooke's Law), this is not the case. For 4.3(a), this uniform field reflects the absence of wall deformation; each segment experiences the full normal reaction dictated by purely kinematic constraints. The consequences of this rigid confinement are evident in Fig. 4.4. Fig. 4.4(a) shows that the robot develops the largest peak normal forces under rigid conditions, with maximum instantaneous values approaching 40 N during anchoring phases. These large forces enable strong frictional traction against the borehole wall and therefore maximize anchoring capacity. As a result, Fig. 4.4(b) shows that the robot achieves the fastest forward progression under rigid confinement, progressing a further distance at equal times with minimal backward slip and steady advancement of the center of mass. However, strong anchorage comes at a substantial energetic cost. Fig. 4.5(a) shows that cumulative

mechanical work increases most rapidly in the rigid case, indicating the highest energy expenditure. Because the wall cannot deform, energy losses occur primarily through frictional slip and repeated high-force interactions with the boundary. This behavior is further quantified in Fig. 4.5(b), where the rigid case exhibits the highest instantaneous COT, corresponding to the steepest work–distance slope. While rigid confinement maximizes propulsion, it represents an energetically expensive and idealized upper bound on performance.

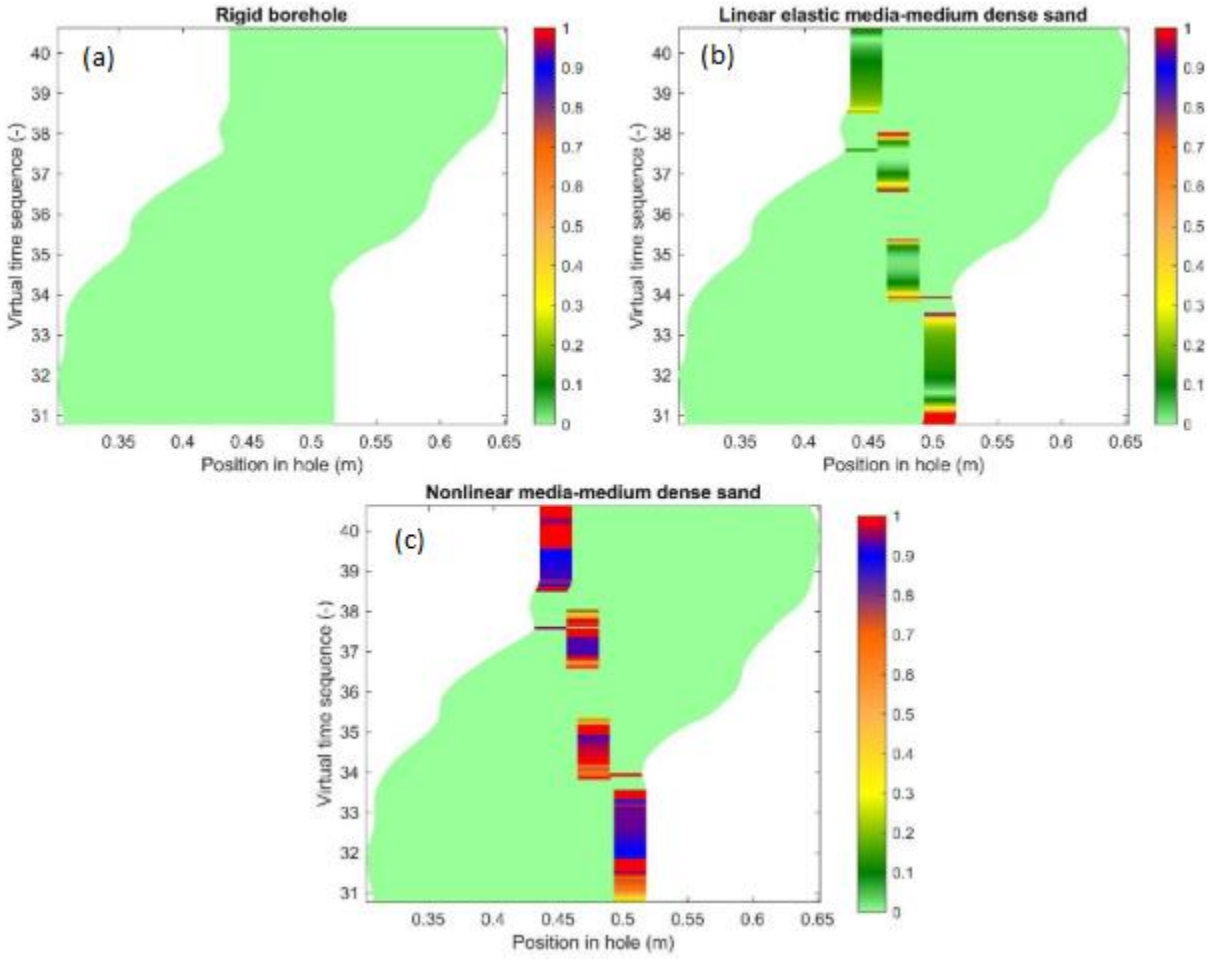

Fig. 4.3. Comparison of normal force ratio (NFR) during locomotion in medium-dense Toyoura sand simulated as a) Rigid media, b) Linear-elastic media, and c) Non-linear media.

Introducing linear soil elasticity allows the borehole wall to deform proportionally to the applied contact force, partially relaxing the rigid kinematic constraint. These results are included to comparatively depict differences in locomotion performance flexible media of constant media stiffness vs. flexible media stiffness determined through an iterative SSI procedure belonging to non-linear behaving media (Fig. 4.3 (c)). This effect is reflected in Fig. 4.3 (b), where localized regions of nonzero NFR appear at axial positions and time steps corresponding to active segment expansion. The NFR values typically reached between 0.2 and 0.4, indicating that a significant fraction of the contact force is absorbed by elastic wall deformation. Compared to the rigid case, Fig. 4.4(a) shows that peak normal forces are moderately reduced, with N_{max} decreasing to approximately 35 N. Despite this reduction, anchoring remains effective, and Fig. 4.4(b) indicates that forward progression of the center of mass is only slightly reduced. The spatial–temporal pattern of force reduction remains relatively smooth and uniform, reflecting the constant tangent stiffness characteristic of linear elasticity. Relative to energy terms, the linear elastic case occupies an intermediate regime compared to rigid media. Fig. 4.4(a) shows a slower accumulation of cumulative work as media transitions to the linear case compared to the rigid wall, as part of the actuation energy is temporarily stored and released through linear wall deformation. Correspondingly, Fig. 4.4(b) indicates a moderate reduction in COT relative to the rigid case. While linear elasticity improves energetic efficiency, it still fails to capture the heterogeneity and stiffness degradation expected in real-world soils under large strains.

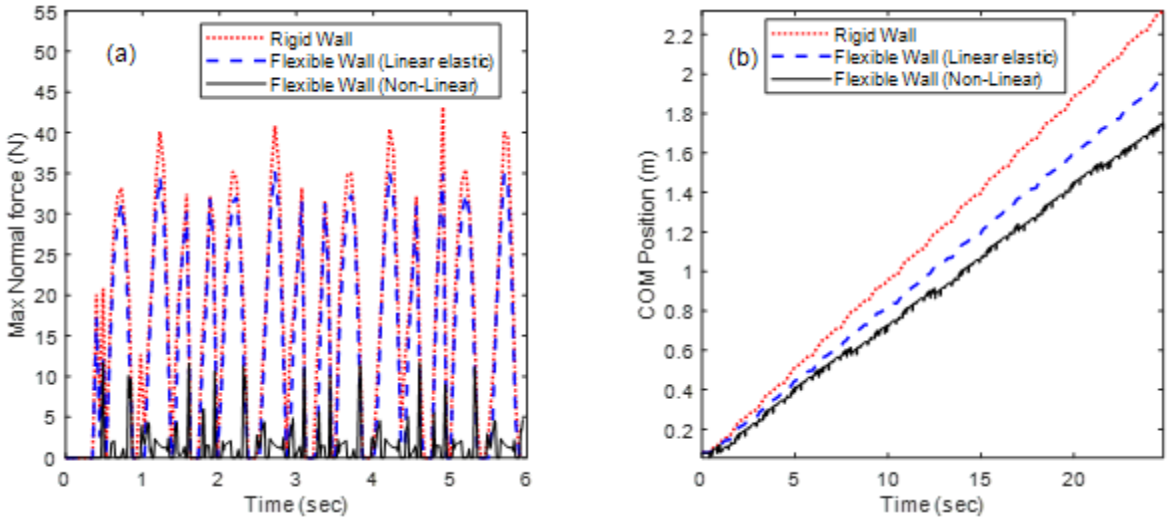

Fig. 4.4. Comparative analysis of locomotion metrics under varying confinement conditions, a) Maximum instantaneous normal force versus time, b) Center-of-Mass (COM) position as a function of time.

The most pronounced changes in robot behavior arise when nonlinear soil stiffness, derived from cavity expansion theory, is introduced. As shown in Fig. 4.3(c), the NFR field becomes highly heterogeneous in both space and time. Extended regions exhibit NFR values between 0.8 and 1.0, particularly during phases of intense segmental compression. These high-NFR zones indicate high magnitudes of reduction in normal force compared to the rigid baseline. This behavior is a direct manifestation of strain-dependent stiffness degradation captured by the nonlinear soil model. As radial expansion increases local strain, the soil's tangent stiffness decreases sharply, allowing large wall deformations to occur with relatively small pressure increases. This response is consistent with a cavity-expansion–like mechanism in which the soil near the boundary becomes highly compliant and partially plastic. The impact on anchoring performance is evident in Fig. 4.4(a), where peak normal forces drop dramatically, often remaining below 10 N. These reduced forces limit the robot's ability to generate frictional traction.

Consequently, Fig. 4.4(b) shows that the nonlinear case exhibits the slowest forward progression seen through the lowest net center-of-mass displacement over the same locomotion interval. Despite weaker anchoring, the nonlinear soil case is energetically favorable. Fig. 4.5(a) shows the lowest cumulative work among all confinement conditions, and Fig. 4.5(b) shows *cost of transport* (COT) in a non-linear flexible wall provides the most efficient motion. Soil compliance absorbs energy, dampens forces, and reduces frictional losses compared to a rigid boundary. This result confirms the lowest work per distance per mass, which is represented by the COT term. The reduction in COT is expected compared to other cases because nonlinear soil deformation absorbs and dissipates a sizable portion of the actuation energy, reducing tangential reaction forces and frictional losses. Softening and damping mechanisms smooth force fluctuations, limiting unnecessary actuator effort even though overall propulsion efficiency is reduced.

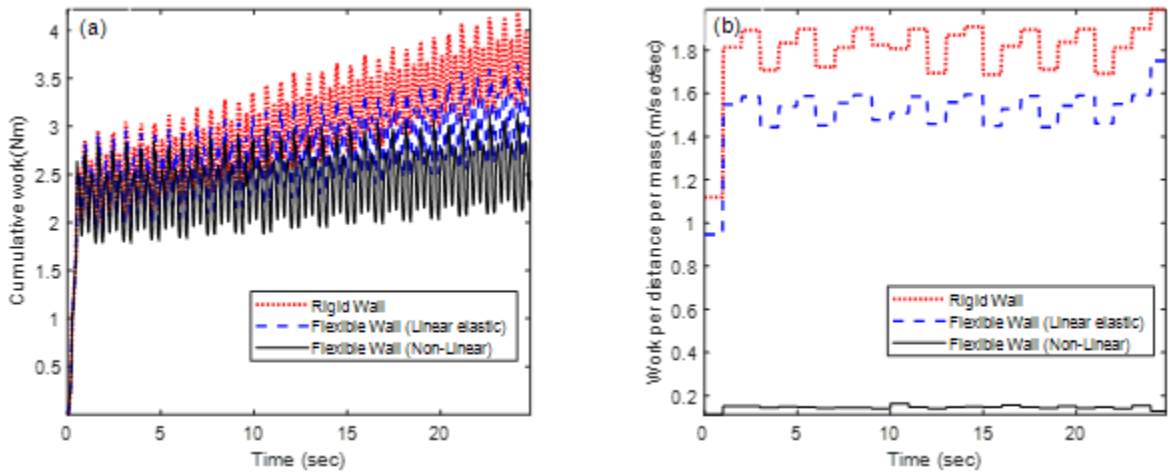

Fig. 4.5. Effect of wall compliance on peristaltic locomotion efficiency, a) Cumulative total work, b) Cost of Transport

4.3 Granular Density as a Determinant of Burrowing Performance

Having established the role of soil stiffness nonlinearity using medium-dense sand as a reference case, we next examine how granular density influences force transmission, anchoring behavior, and energetic efficiency during peristaltic locomotion. This analysis focuses on Toyoura sand under two grain-packing states, dense and loose, while all other robot and actuation parameters are held constant.

Fig. 4.6 presents the spatial–temporal distribution of the Normal Force Reduction (NFR) for dense and loose sand. Clear differences emerge between the two density states. In loose sand, the robot experiences extensive regions of high NFR, frequently exceeding 0.9 in magnitude. These regions coincide with phases of strong segmental expansion, during which the loose granular assembly undergoes a high degree of stiffness degradation and localized yielding. As a result, radial deformation is accommodated by a minimal increase in contact pressure, leading to substantial reductions in normal force relative to the rigid-wall baseline. In contrast, dense sand exhibits broader and more spatially varying regions of moderate magnitudes of NFR, typically ranging between 0.5 and 0.9. The higher initial packing density and increased coordination number of the grains result in a stiffer response, limiting radial deformation and sustaining larger contact forces during anchoring phases. Consequently, stiffness degradation is less severe and more evenly distributed along the body.

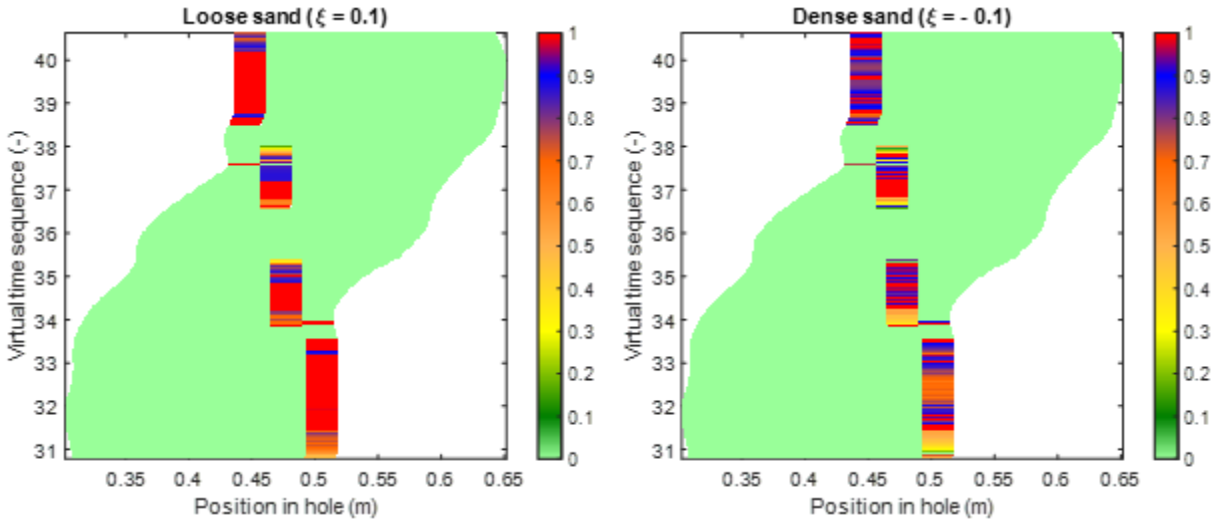

Fig. 4.6. Normal force reduction ratios for earthworm robot locomotion in dense vs. loose nonlinearly behaving sand.

The implications of the medium density on locomotion are quantified in Fig. 4.7. Fig. 4.7(a) shows the evolution of the maximum instantaneous normal force, N_{max}, over time. Dense sand consistently produces higher peak normal forces during each actuation cycle, reflecting its greater confinement stiffness and enhanced resistance to radial expansion. These higher forces improve anchoring reliability but require increased actuation effort. In loose sand, the reduced stiffness leads to substantially lower force peaks, indicating weaker anchorage corresponding to higher degrees of local deformation as well as diminished load transfer to the surrounding medium. Fig. 4.7(b) presents the corresponding cost of transport (COT), defined as the work performed per unit distance and mass. Despite weaker anchoring force seen in 4.7(a), locomotion in loose sand yields a lower overall COT, indicating higher energy efficiency. This reduction in energetic cost arises from decreased normal forces, reduced frictional resistance, and lower slip-related energy losses. Dense sand, while providing stronger anchoring and improved thrust generation, incurs a higher energetic penalty due to the increased work required to overcome soil

resistance.

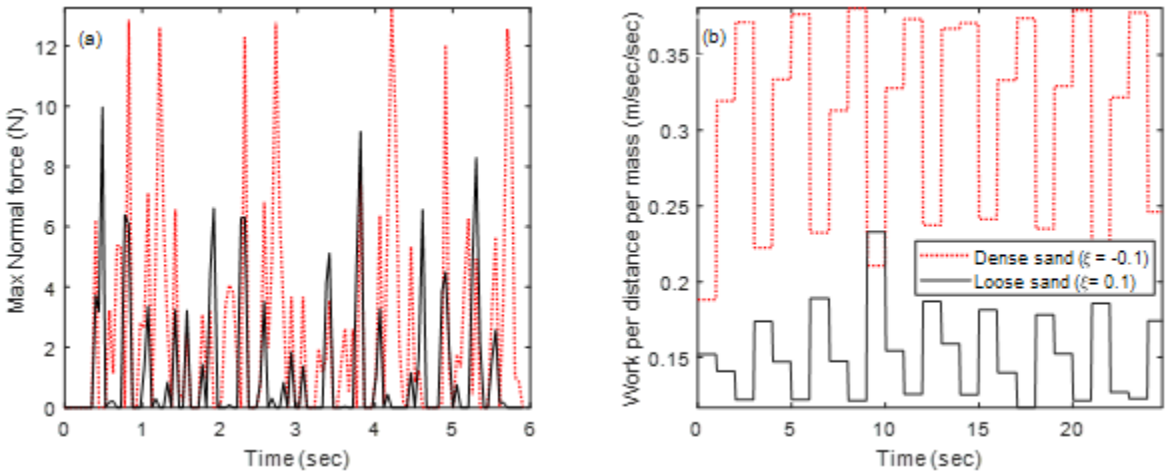

Fig. 4.7. Effect of sand density on peristaltic locomotion, a) Maximum normal force evolution, and b) Density-dependent trends in Cost of Transport.

Fig. 4.8 further clarifies this trend by examining the maximum tangential force generated instantaneously under loose, medium-dense, and dense sand conditions. Tangential force is governed by the Coulomb relation $T=\mu*N$, where the friction coefficient μ is prescribed as 0.8 for dense sand, 0.65 for medium-dense sand, and 0.5 for loose sand. As expected, though dense sand peaks are highly varied, the figure exhibits the largest tangential force peaks, with instantaneous magnitude frequently reaching 9–11 N. These values are approximately 1.6–1.8 times larger than those observed in medium-dense sand, where peak forces remain mostly within 5–7 N, and more than twice those measured in loose sand, which rarely exceed 4–5 N. These magnitudes here reflect the combined effects of higher normal forces (reviewed in Fig. 4.7(a)) and the higher magnitude friction coefficient as assigned to higher densities, resulting in strong frictional coupling and effective anchoring during contraction phases and showing density-dependent differences in peak magnitude and intermittency. The medium-dense sand response lies between the two extremes. Compared to dense sand, the peak tangential force is reduced by approximately 30–40%,

consistent with the lower friction coefficient (μ=0.65) and moderate normal force levels. Nevertheless, it is believed these force magnitudes derived from medium-dense sand remain sufficient to support reliable anchoring, while the reduced peak amplitudes indicate both reduced resistance to forward motion and less pronounced stick–slip behavior. In contrast, loose sand produces the lowest tangential force levels, with maxima typically below 3 N. Tangential force magnitudes only sporadically approached 5 N. Relative to dense sand, this corresponds to a 60–70% reduction in peak tangential force. The low friction coefficient (μ=0.5), combined with substantial normal force reduction due to granular yielding (illustrated in Fig. 4.7), limits the transferable shear force at the interface of the borehole wall. While this weakens anchoring capabilities and increases slip during thrust phases, it significantly reduces frictional energy dissipation, contributing to the lower COT reported in Fig. 4.7(b).

Taken together, these results demonstrate that granular density controls peristaltic locomotion primarily through its influence on dilation, effective stress evolution, and confinement stress. Dense sands improve anchoring capability and thrust but comes with a higher cost of energy, whereas loose sands reduce energy demand but limits transferable shear force and leads to lower propulsion efficiency.

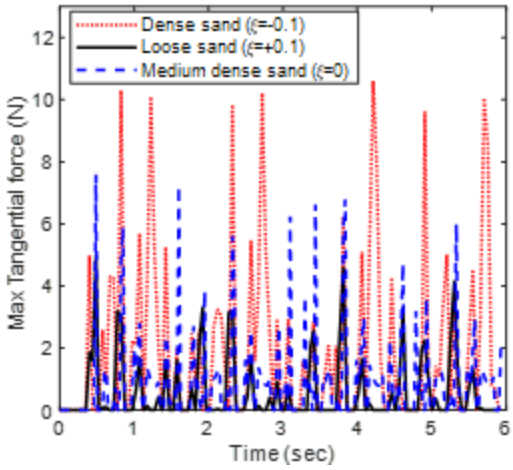

Fig. 4.8. Time history of maximum tangential force for dense, medium-dense, and loose sand.

4.4 Soil Stiffness Effects on Peristaltic Locomotion in Fine-Grained Soil

Fine-grained soils introduce additional dominance over peristaltic locomotion that are not present in previously studied, coarse-grained sands, primarily due to their stress history (related to consolidation) and drainage behavior. Fine-grained soils of focus here are clays and silts. In clays, mechanical response is strongly governed by pre-consolidation history, while in silts, the degree of drainage during cyclic loading plays a dominant role. These factors directly influence soil stiffness, effective stress evolution, and the ability of the surrounding medium to sustain contact pressures with little deformation/local failure during segment actuation.

The influence of stress history is examined using clays with over-consolidation ratios (OCR) of 1 and 8. Fig. 4.9 shows the spatial–temporal evolution of the Normal Force Reduction (NFR) for these two cases. In normally consolidated clay (OCR = 1), NFR values remain close to unity over most of the locomotion cycle, indicating rapid stress relaxation and more soil compliance. Segmental expansion induces local yielding, meaning the soil deforms with minimal increase in contact pressure required. This results in weaker reaction forces, limited anchoring

capacity, and generation of thrust. In contrast, the highly over-consolidated clay (OCR = 8) exhibits substantially lower NFR values, often near 0.55, reflecting a stiffer response in which contact pressures are sustained over time. The higher pre-consolidation stress increases the elastic range and suppresses early yielding, allowing larger normal forces to develop during anchoring phases. These trends confirm that clay stress history directly controls force transmission and energetic efficiency during peristaltic locomotion.

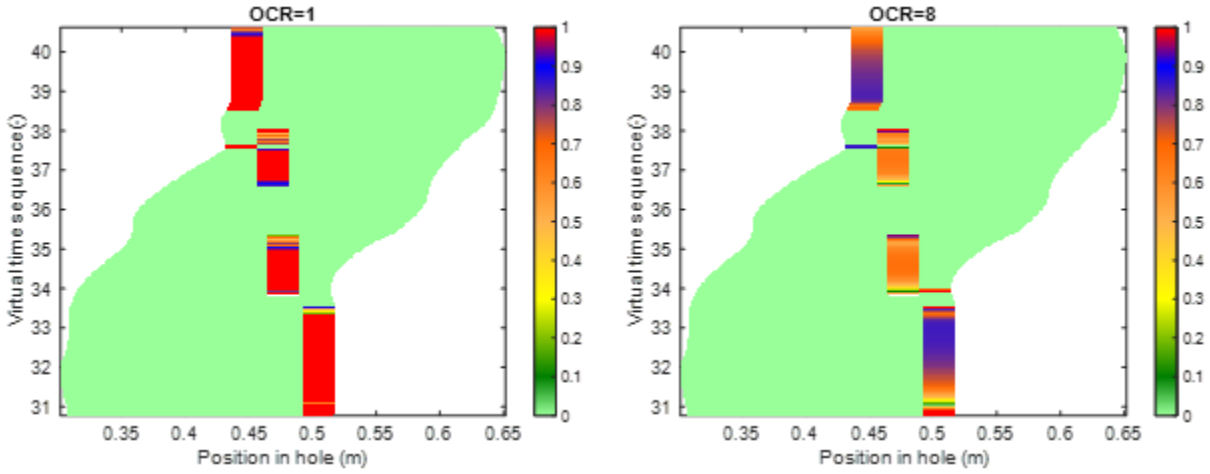

Fig. 4.9. Normal force reduction ratios for clays at over-consolidation ratios OCR = 1 and 8.

These effects are quantified further in Fig. 4.10. Fig. 4.10(a) shows that increasing OCR leads to higher peak values of the maximum normal force, N_{max}, with sharper and more persistent force peaks in the over-consolidated case. As seen in other cases, Fig. 4.10(b) shows that the cost of transport (COT) also increases with OCR, reflecting the greater mechanical work required to impose the same expansion amplitude shown in other cases for stiffer clay. Although the increase in energy demand is known, the improved anchoring in over-consolidated clay enables greater net advancement per cycle during locomotion, partially offsetting the higher cost of energy. In

normally consolidated clay, lower energy input is required, but weak confinement limits effective propulsion.

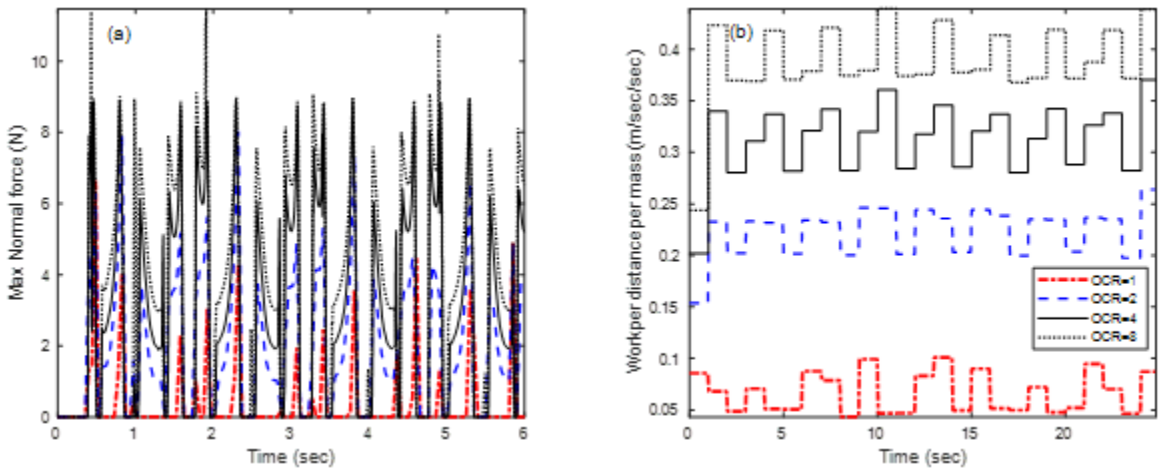

Fig. 4.10. Effect of clay over-consolidation ratio on aspects of peristaltic locomotion, a) Maximum normal force evolution, and b) Density-dependent trends in Cost of Transport.

For silts, drainage conditions impose a stronger influence than stress history on aspects of locomotion due to their intermediate permeability and sensitivity to pore pressure generation during cyclic loading. Fig. 4.11 compares NFR distributions for undrained medium-dense silt, drained medium-dense silt, and drained dense silt, respectively. Under undrained conditions, rapid segmental expansion generates excess pore pressures that cannot dissipate within each actuation cycle. This assertion agrees with laboratory phenomenon, where rapid loading generates excess pore pressures as well. The resulting reduction in effective stress leads to pronounced degradation of stiffness (soil softening), with NFR values remaining close to unity. At the same rate, normal stresses relax rapidly, limiting anchoring capacity despite the lowered cost of energy to deform the soil. When drainage is permitted, pore pressures dissipate between cycles, increasing effective

stress and mobilized stiffness. This results in lower NFR values seen in and improved confinement, particularly in the drained dense silt shown in Fig. 11(c), which exhibits the lowest NFR.

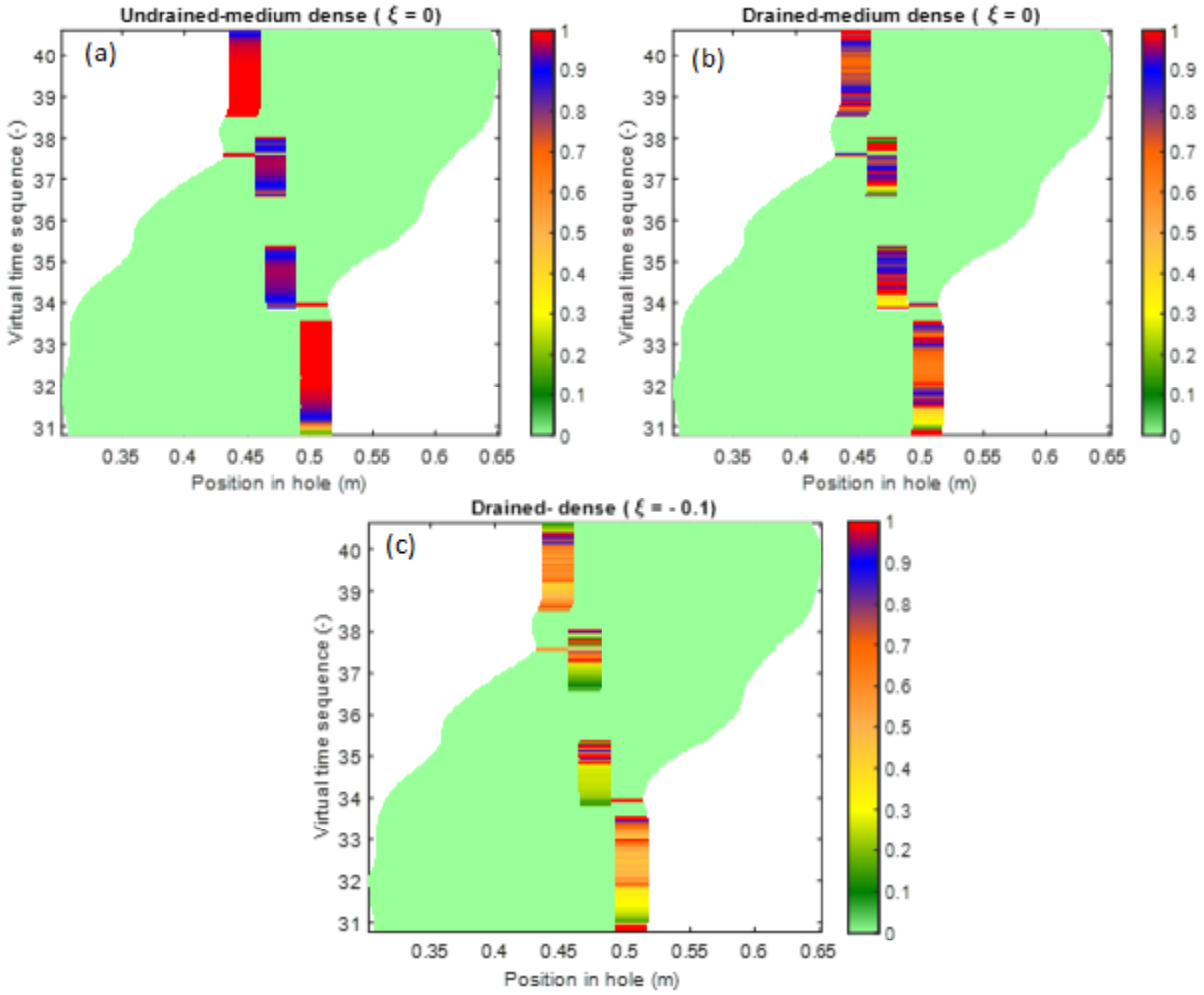

Fig. 4.11. Normal force ratio comparison for silt under a) undrained, b) drained (medium dense), and c) drained (dense) conditions.

Fig. 4.12 illustrates the corresponding force and energy trends. Fig. 4.12(a) shows that drained dense silt produces the highest and sharpest peaks in N_{max}, indicating strong confinement and effective anchoring. The drained medium-dense case periodically exhibits intermediate levels of force magnitude, while the undrained case produces consistently lower forces. Fig. 4.12(b)

shows that these stiffness differences translate directly into energetic performance, seen in many other instances of this study. The undrained case yields the lowest COT due to minimal resistance, but suffers from less anchorage and reduced thrust. The drained, dense silt incurs the highest COT, reflecting the increased work required to deform a stiff, well-drained soil for adequate anchorage. These results demonstrate that drainage and density jointly control both force transmission and energetic efficiency during peristaltic locomotion in silts.

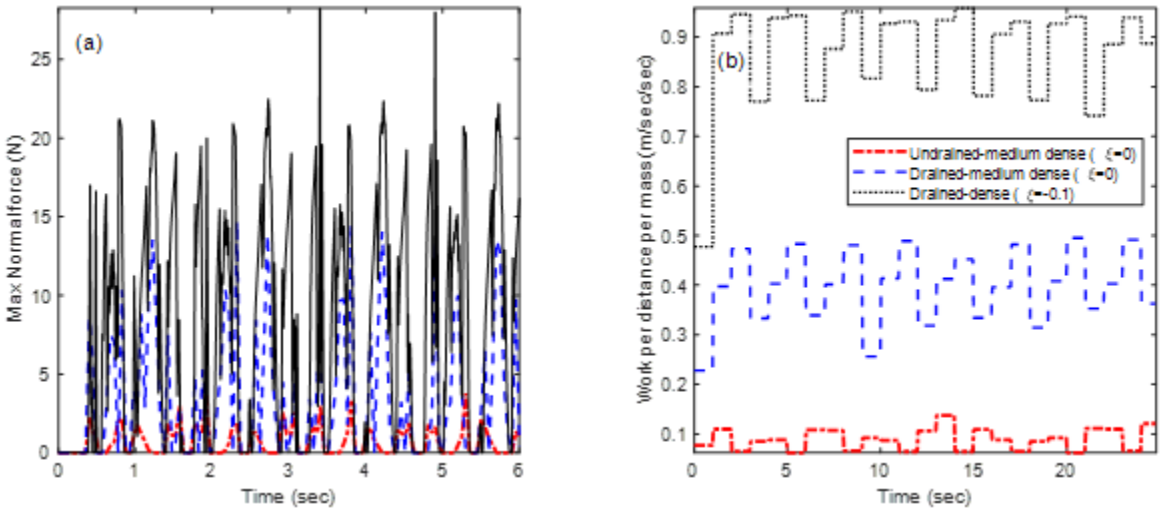

Fig. 4.12. Effect of the drainage boundary condition and stiffness of the silty soil on locomotion, a) Maximum normal force evolution and b) Density-dependent trends in Cost of Transport.

4.5 Effects of Robot Stiffness on Locomotion Performance

The influence of robot axial stiffness on contact mechanics, propulsion, and energetic efficiency is examined in Fig. 4.13. In all simulations, the surrounding soil is modeled as medium-dense sand under drained conditions, and all robot and soil parameters except axial stiffness are held constant. This setup isolates the role of robot compliance in governing measurable parameters of soil–robot interaction and locomotion performance. For Fig. 18 simulations, four stiffness levels are considered: K (baseline, K = 13.5 N/m), 0.5K, 1.5K, and 2K.

Fig. 4.13(a) shows the peak instantaneous normal force acting on the robot segments. The most compliant/axially least stiff robot (0.5K) exhibits large and intermittent force peaks, reaching approximately 15 N. These peaks arise from excessive segmental deformation during actuation, which concentrates contact forces at a limited number of anchoring locations. As stiffness increases toward the baseline value and beyond to 1.5 and 2K, the peak normal forces decrease and become more evenly distributed in time, indicating more stable and sustained anchoring. In contrast, the stiffest configuration (2K) generates consistently low normal forces, reflecting insufficient radial deformation to engage the borehole wall effectively.

The impact of stiffness on locomotion kinematics is illustrated by the COM trajectories in Fig. 4.13(b). Over the simulated interval, the compliant robot (0.5K) achieves the largest net forward displacement, corresponding to a higher apparent locomotion speed. This behavior results from large body deformations that enable aggressive extension phases and slip-assisted advancement. However, this motion is achieved through unstable and highly localized anchoring and does not represent efficient force transmission. The baseline (K) and moderately stiff (1.5K) configurations exhibit slightly slower but more controlled progression, offsetting less net forward progression over the same time for a balance between deformation and anchoring. The stiffest robot (2K) advances the least, as inadequate contact prevents effective thrust generation.

Fig. 4.13(c) presents the cumulative mechanical work input, which shows relatively minor variation across stiffness levels. This similarity indicates that cumulative work alone is insufficient in characterizing locomotion efficiency. A clearer distinction emerges when the work is normalized by distance and mass in terms of COT, shown in Fig. 4.13(d). The baseline stiffness K exhibits the second highest COT among physically effective locomotion regimes, reflecting a

favorable balance between compliant deformation and stable anchoring. The compliant robot (0.5K) shows a more reduced COT due to its larger forward displacement; however, this apparent efficiency is accompanied by excessive deformation, intermittent contact, and increased slip, indicating a less robust locomotion mode.

The stiffest configuration (2*K*) displays the lowest apparent COT, but this result is misleading. In this case, insufficient radial deformation prevents consistent contact with the borehole wall, leading to lack of anchorage in this simulation. Since COT is computed from cumulative slip dissipation, reduced contact forces artificially lower frictional work, producing a deceptively low COT. This regime therefore represents a non-functional locomotion state rather than an optimized design. The results demonstrate that COT must be interpreted in conjunction with anchoring quality and forward progression to avoid false performance optima.

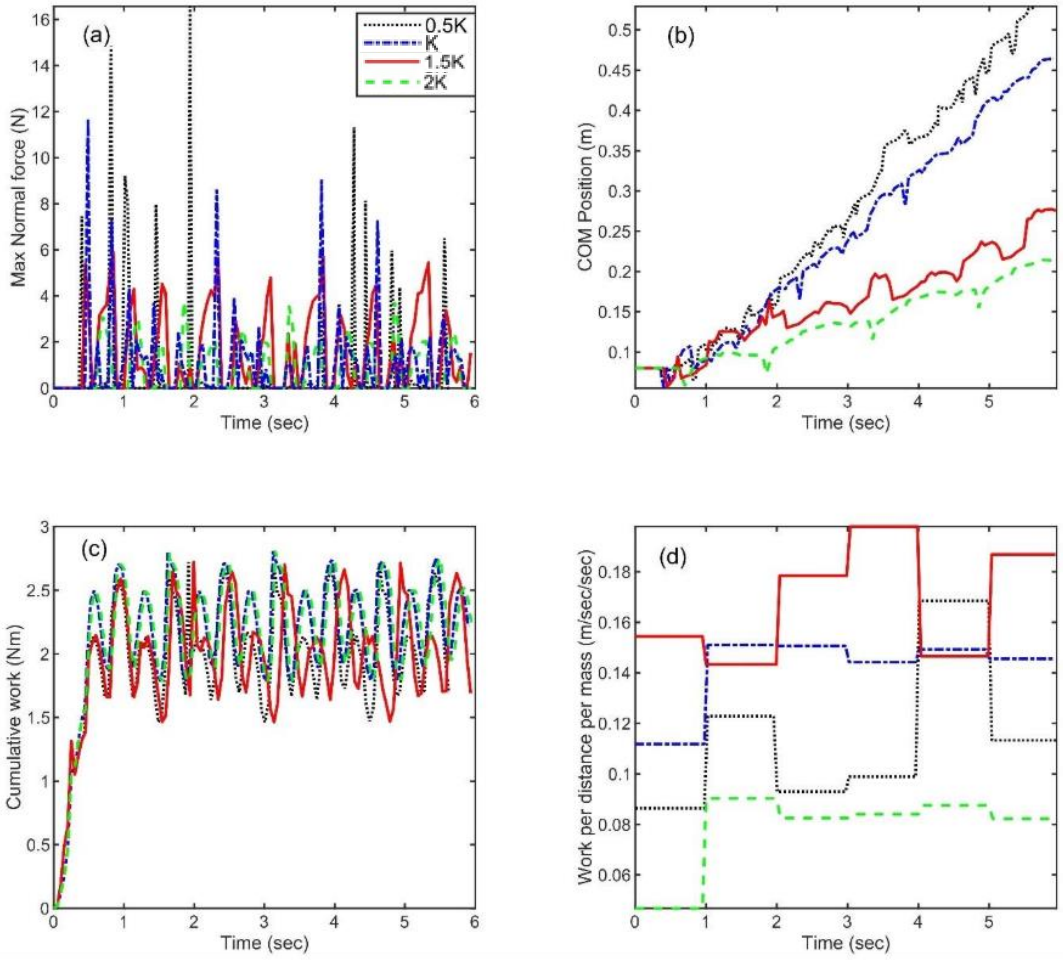

Fig. 4.13. Influence of robot axial stiffness on locomotion performance, a) peak normal force, b) center-of-mass progression, c) cumulative mechanical work, and d) cost of transport for stiffness values $0.5K$, K, $1.5K$, $2K$.

4.6 Verification of Analytical Framework

Verification of the SSI analytical framework was conducted to assess the accuracy of tabulated results compared to a high-fidelity Finite Element Method (FEM) solution. The verification was conducted in three steps: discrete model response extraction, FEM validation in Abaqus/Standard FEA software, and comparative analysis of results and validation.

Discrete model response extraction involved simulating the burrowing environment as an elastic soil medium with a radial stiffness, k, equating to 10,000 N/m. Linear elastic media was simulated compared to convoluted elastic-plastic media for simplicity in later numerical analysis. Instantaneous normal contact force magnitudes issued by segments in contact with the borehole and spatial distribution of such for each timestep were extracted from the results. Once plotted against time, the peak normal contact force curves captured the localized contact and loading progression along the robot body during peristaltic locomotion. Those results are shown in Fig. 4.14.

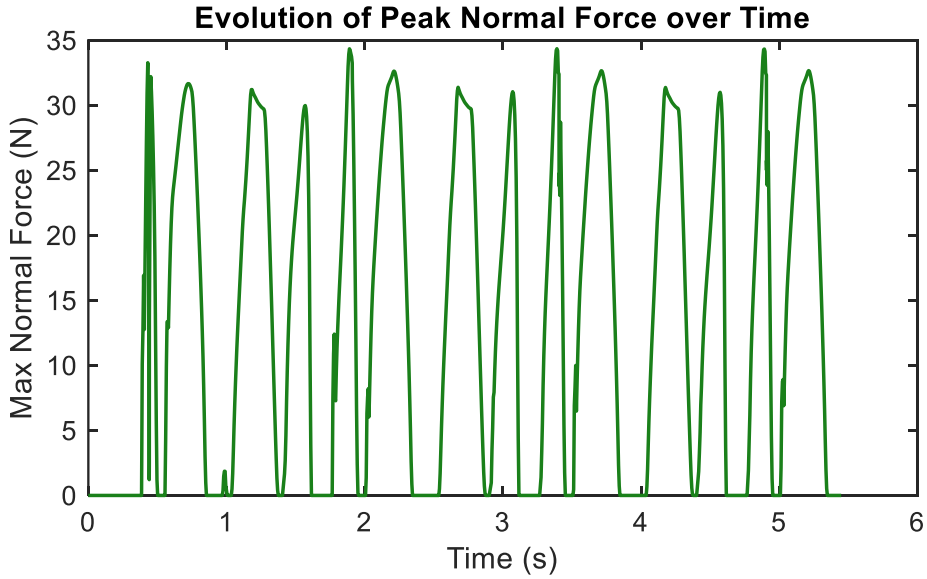

Fig. 4.14. Resulting contact mechanics by simulated peristaltic locomotion.

FEM validation in Abaqus required validation of the SSI formulation of discrete, independent springs, such that an independent numerical model was developed in the software. The soil domain was modeled as a 3D linear elastic media, consistent with step 1 of the verification process. Boundaries were created to be sufficiently large to ensure no boundary effects, setup of the soil domain depicted in Fig. 4.15.

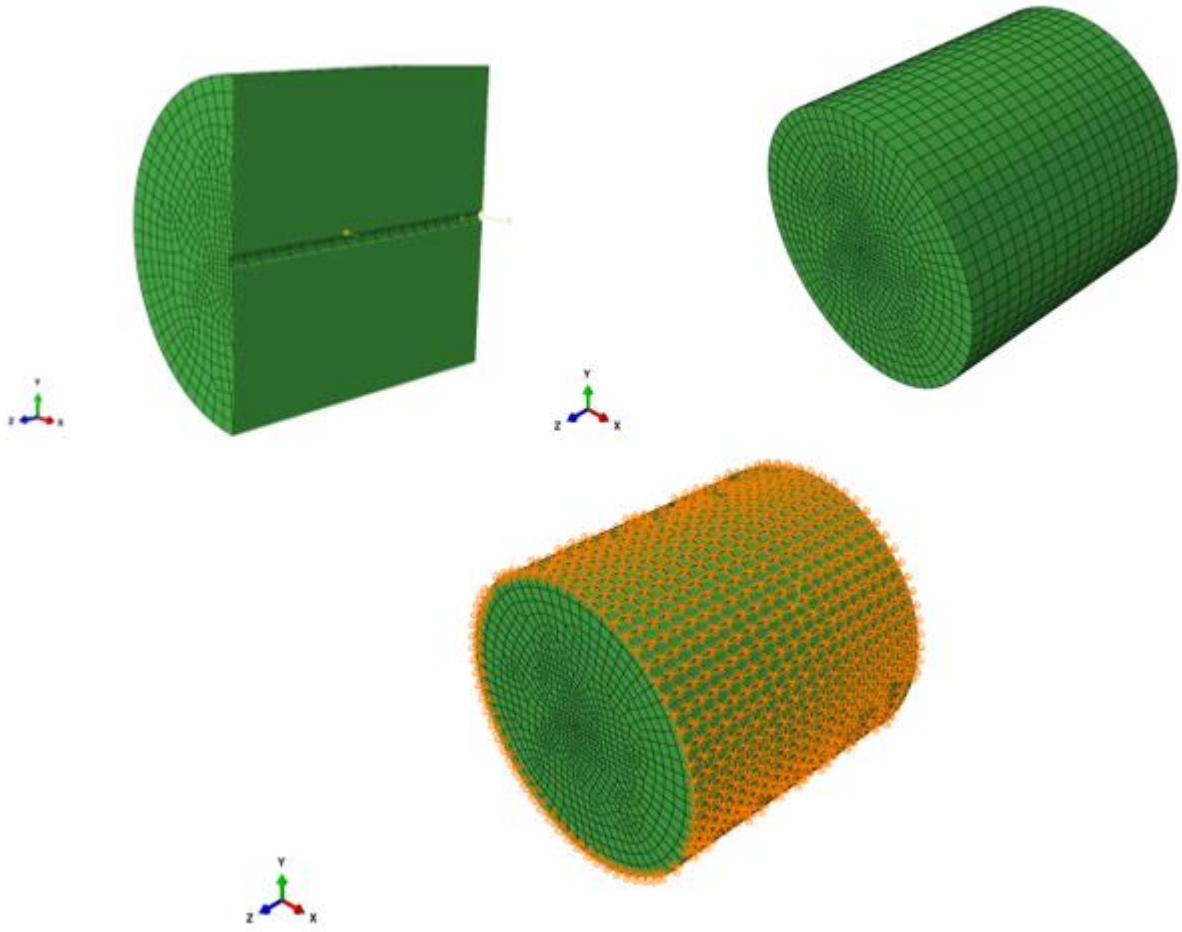

Fig. 4.15. 3D Finite Element Model (FEM) Configuration in Abaqus representing the soil media used in burrowing.

Comparison of results between the analytical framework and FEM analysis are depicted in Fig. 4.16. Comparison between the two models begins with denoting borehole wall deformation, (ΔH), as a function of position. Both models exhibit spatial trends with deformation concentrated near areas of peak contact force and gradually diminishing away from loading zones. Magnitude and spatial distribution similarities confirm that the analytical framework correctly captures soil deformation within simulations. FEM simulations consistently produced lower peak normal contact forces, meaning a stiffer response. This was due to differences between the two modeling

approaches, soil in the FEM simulation being a 3D, continuous media allowing stress and deformation to propagate throughout the soil volume. Where the region is larger, more soil material participates in resisting the applied loads, resulting in a stiff response depicted in Fig. 4.16.

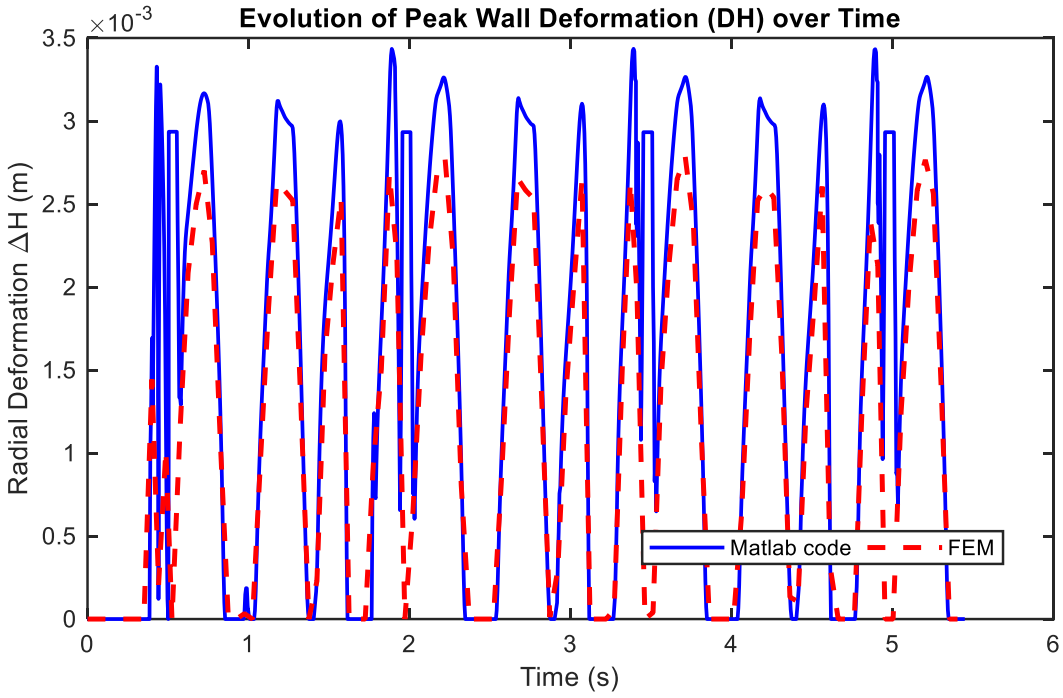

Fig. 4.16. Comparison of Radial Borehole Wall Deformation between MATLAB SSI Model and 3D FEM approximation.

Chapter 5: Summary, Conclusions, and Recommendations

5.1 Summary

Bio-inspired robots are quickly becoming a viable option within our built infrastructure. Their ability to install, repair, and provide other uses are continuously being developed and refined to reach new areas of infrastructure. Geotechnical engineering is a direct application of such technology. These robots possess the ability to perform site characterization of in-situ soil and monitor environmental conditions in and around our built infrastructure. One challenge within geotechnical engineering is the ability to access subsurface infrastructure such as utility lines in densely populated, urban areas. Mobilizing drill rigs and other heavy machinery to these areas is costly and poses a risk of disturbing subsurface conditions of nearby infrastructure. Bio-inspired robots may be key in addressing such issues, where such technology limits ground disturbance, is less costly to mobilize, and can perform tasks in harsh environments. One issue in developing undergrounding robots is testing their capabilities in various soil types and conditions. This study addresses such an issue, enabling conclusions to be drawn regarding locomotion performance in realistic soils of varying densities, stress history, and drainage conditions, which highlights a reduction in manual labor and costs associated with laboratory testing in future research in robot performance within similar burrowing environments.

In this work, robot peristaltic locomotion performance was characterized based on simulation results of a modified analytical framework originally introduced by Mills et al. (2025) and builds upon the foundational concepts originally proposed by Daltorio et al. (2013). The program originally modeled movement and mechanisms of a segmented, biologically inspired, peristaltic robot in rigid media. This framework was expanded from rigid media to one with compliant, deformable boundaries. This improvement includes incorporating soil structure

interaction concepts and cavity expansion theory to model the nonlinear behavior between force and displacement of a radially expanding, cylindrical subsurface cavity, best and most simply illustrated through Hooke's Law. Soil–structure interaction was modeled using discrete nonlinear radial springs whose force–displacement relationships are derived from cylindrical cavity expansion theory, which was done in order to capture strain-dependent stiffness degradation, yielding, and stress-history effects without resorting to full continuum or particle-scale simulations. CET captures elastic–plastic deformation, stiffness degradation, and the evolution of confining pressure during cavity expansion by solving coupled stress-strain fields around the cavity.

The process included performing cavity expansion analysis using ASCEND, a program developed by Jaeger (2018) based on the semi-analytical formulations for drained and undrained cylindrical cavity expansion. After force and displacement relationships for individual timesteps were tabulated from ASCEND simulations, where a parametric study plan regarding cavity expansion within varying density, drainage conditions, and stress history in Toyoura sand, Silica flour, and Boston Blue Clay, was executed, results were incorporated back into the modified analytical framework for another set of simulations that models interaction between robot locomotion and the now deformable media that behave under cavity expansion theory. Subsequent results from simulations were obtained that represents varying magnitudes of NFR, a normalized measure of the reduction in reaction normal force resulting from radial expansion into compliant borehole walls, maximum instantaneous normal force, N_{max}, and COM as a function of time, cumulative work, and cost of transport (work per distance per mass). The effect of varying magnitudes of the axial stiffness belonging to the simulated robot on such metrics were parametrically studied, reported, and discussed as well.

5.2 Conclusion

From this study, the following conclusions were made:

- Normal Force Reduction (NFR) was an excellent method for initial characterization of how reaction force magnitude varied under a range of soil types, drainage conditions, and stress history, as well as axial robot stiffness, when boreholes were subjected to radial stress
- Nonlinearly behaving soils possessed the highest magnitude of reduction in reaction normal force. Paired with results showing significantly lower N_{max} values, cumulative work, and COT, it is concluded that this evidence offsets the robot's lesser COM position as a function of time compared to simulations in rigid and linear media cases.
- Regarding simulation results in Toyoura sand, NFR ratios were highest in expanding cavities within loose sand. N_{max} peaks, tangential force peaks, and COT were significantly higher in dense sands as well. It is concluded that, should the user desire energy-efficient locomotion, loose sand should be used in experimentation, while dense sand should be used if better anchorage and thrust capabilities are desired. Medium dense sand could provide desirable results for both qualities.
- Regarding simulation results in Boston Blue Clay, NFR ratios were highest in expanding cavities within lower stress-state clays (e.g., NC clay). While high OC clay (OC = 8) still provided favorable reduction in force for some timesteps, lower OC clays possessed best results for minimizing magnitudes of reaction force as well as significantly lower COT. It is concluded that, should the user desire testing in clays/soils with high clay content, lower OC clays provide more energy-efficient results, while higher OC clays will provide robots better anchorage and thrust capabilities.

- Regarding simulation results in Silica flour, NFR ratios were highest in expanding cavities in less dense silts. Further examination showed that while drainage impacted N_{max} magnitudes, which can be seen less obviously from NFR figures, locomotion COT was far lower in both drained and undrained, medium-dense silt. It is concluded that, should the user desire testing in silt-like soils, density of the medium will factor into producing lower reaction forces during locomotion. Dense, silt-like mediums will require a higher COT but will aid in producing greater anchoring and thrust capabilities.
- Regarding simulation results from ranging the robot axial stiffness coefficient, results showed favorable results for stiffnesses at both default and 1.5x default magnitude. This is evidenced in both N_{max} peaks and COM curves as a function of time, where results for these were between maximum cases 0.5x and 2.0x stiffness. Furthermore, it is concluded that cumulative work and COT metrics alone are not adequate in characterizing robot stiffness effects on locomotion performance.

5.3 Recommendations

Following the conclusion of this study, the following recommendations are made for future work:

- Collaborate with ASCEND creator(s) to import MIT-S1 directly into MATLAB program.
- Experimentally test segmented robot in built subsurface environment to physically validate reaction forces obtained from respective simulations in this work.
- Develop a displacement control actuator for robot locomotion which can make the model more suitable for numerical verification.
- Perform analyses to optimize design of the robot before proceeding to computationally expensive numerical or financially expensive experimental studies.

References

Abell, J. A., Orbović, N., McCallen, D. B., & Jeremic, B. (2018). Earthquake soil-structure interaction of nuclear power plants, differences in response to 3-D, 3 × 1-D, and 1-D excitations. *Earthquake Engineering & Structural Dynamics, 47(6), 1478–1495.* https://doi.org/10.1002/eqe.3026

Alexander, R. M. (1982). *Locomotion of animals.* Glasgow: Blackie.

Alexander, G., Almendinger, J., & White, P. (2022). The long-term effects of invasive earthworms on plant community composition and diversity in a hardwood forest in northern Minnesota. *Plant-Environment Interactions*, *3*(2), 89–102. https://doi.org/10.1002/pei3.10075

Alqadad, A., Shahrour, I., & Sukik, A. (2017). Smart system for safe and optimal soil investigation in urban areas. Underground Space, 2(4), 220-226. https://doi.org/10.1016/j.undsp.2017.10.003

Ansell, A. D., & Nair, N. B. (1969). The mechanisms of boring in Martesia striata Linné (Bivalvia: Pholadidae) and Xylophaga dorsalis Turton (Bivalvia: Xylophaginidae). Proceedings of the Royal Society of London. Series B. Biological Sciences, 174(1034), 123–133. https://doi.org/10.1098/rspb.1969.0084

Bapir, B., Abrahamczyk, L., Wichtmann, T., & Prada-Sarmiento, L. F. (2023). Soil-structure interaction: A state-of-the-art review of modeling techniques and studies on seismic response of building structures. *Frontiers in Built Environment*, *9*, 1120351. https://doi.org/10.3389/fbuil.2023.1120351

Bi, Z., Zhou, Q., & Fang, H. (2023). A worm-snake-inspired metameric robot for multi-modal locomotion: Design, modeling, and unified gait control. International Journal of Mechanical Sciences, 254, 108436. https://doi.org/10.1016/J.IJMECSCI.2023.108436

Bishop, R. F., Hill, R., & Mott, N. F. (1945). The theory of indentation and hardness tests. *Proceedings of the Physical Society*, *57*(3), 147–159. https://doi.org/10.1088/0959-5309/57/3/301

Boxerbaum, A. S., Shaw, K. M., Chiel, H. J., & Quinn, R. D. (2012). Continuous wave peristaltic motion in a robot. *The International Journal of Robotics Research*, *31*(3), 302–318. https://doi.org/10.1177/0278364911432486

Briaud, J. (2023). *Geotechnical Engineering* (1st ed.). Wiley. https://doi.org/10.1002/9781119788720

Carbonari, S., Morici, M., Dezi, F., Gara, F., & Leoni, G. (2017). Soil-structure interaction effects in single bridge piers founded on inclined pile groups. *Soil Dynamics and Earthquake Engineering*, *92*, 52–67. https://doi.org/10.1016/j.soildyn.2016.10.005

Carter, J. P., Booker, J. R., & Yeung, S. K. (1986). Cavity expansion in cohesive frictional soils. *Géotechnique*, *36*(3), 349–358. https://doi.org/10.1680/geot.1986.36.3.349

Chen, S. L., & Abousleiman, Y. N. (2012). Exact undrained elasto-plastic solution for cylindrical cavity expansion in modified Cam Clay soil. *Géotechnique*, *62*(5), 447–456. https://doi.org/10.1680/geot.11.P.027

Chen, S. L., & Abousleiman, Y. N. (2013). Exact drained solution for cylindrical cavity expansion in modified Cam Clay soil. *Géotechnique*, *63*(6), 510–517. https://doi.org/10.1680/geot.11.P.088

Chen, S. L., & Abousleiman, Y. N. (2018). Cavity expansion in strain hardening frictional soils under drained condition. *International Journal for Numerical and Analytical Methods in Geomechanics*, *42*(1), 132–142. https://doi.org/10.1002/nag.2718

Chen, Y., Khosravi, A., Martinez, A., & Dejong, J. (2021). Modeling the self-penetration process of a bio-inspired probe in granular soils. *Bioinspiration and Biomimetics*, *16*(4). https://doi.org/10.1088/1748-3190/abf46e

Chen, Y., Martinez, A., & Dejong, J. (2022). DEM study of the alteration of the stress state in granular media around a bio-inspired probe. *Canadian Geotechnical Journal, 59(10)*. https://doi.org/10.1139/cgj-2021-0260

Chen, Y., Zhang, N., Fuentes, R., & Martinez, A. (2024). A numerical study on the multi-cycle self-burrowing of a dual-anchor probe in shallow coarse-grained soils of varying density. *Acta Geotechnica, 19(3)*. https://doi.org/10.1007/s11440-023-02088-9

Civelekler, E., Okur, V. D., & Afacan, K. B. (2021). A study of the local site effects on the ground response for the city of Eskişehir, Turkey. *Bulletin of Engineering Geology and the Environment*, *80*(7), 5589–5607. https://doi.org/10.1007/s10064-021-02285-4

Crane, R. L., & Merz, R. A. (2017). Mechanical properties of sediment determine burrowing success and influence distribution of two lugworm species. *Journal of Experimental Biology*, *220*(18), 3248–3259. https://doi.org/10.1242/jeb.156760

Daltorio, K. A., Boxerbaum, A. S., Horchler, A. D., Shaw, K. M., Chiel, H. J., & Quinn, R. D. (2013). Efficient worm-like locomotion: Slip and control of soft-bodied peristaltic robots. *Bioinspiration & Biomimetics*, *8*(3), 035003. https://doi.org/10.1088/1748-3182/8/3/035003

Das, B. M. (2007). *Fundamentals of geotechnical engineering* (3rd ed.). Thomson Brooks/Cole.

Dorgan, K. M., Jumars, P. A., Johnson, B., Boudreau, B. P., & Landis, E. (2005). Burrow extension by crack propagation. *Nature*, *433*(7025), 475–475. https://doi.org/10.1038/433475a

Dorgan, K. M., Arwade, S. R., & Jumars, P. A. (2007). Burrowing in marine muds by crack propagation: Kinematics and forces. *Journal of Experimental Biology*, *210*(23), 4198–4212. https://doi.org/10.1242/jeb.010371

Dorgan, K. M. (2015). The biomechanics of burrowing and boring. *The Journal of Experimental Biology*, *218*(Pt 2), 176–183. https://doi.org/10.1242/jeb.086983

Dorgan, K. M. (2018). Kinematics of burrowing by peristalsis in granular sands. *Journal of Experimental Biology*, jeb.167759. https://doi.org/10.1242/jeb.167759

Drew, G. A. (1907). THE HABITS AND MOVEMENTS OF THE RAZORSHELL CLAM, ENSIS DIRECTUS, CON. *The Biological Bulletin*, *12*(3), 127–140. https://doi.org/10.2307/1535859

Dutta, S. C., & Roy, R. (2002). A critical review on idealization and modeling for interaction among soil–foundation–structure system. *Computers & Structures*, *80*(20–21), 1579–1594. https://doi.org/10.1016/S0045-7949(02)00115-3

Elder, H.Y. & Trueman, E.R., editors. (1980). Aspects of Animal Movement, 250 pp. Cambridge University Press. *Journal of the Marine Biological Association of the United Kingdom*, *61*(2), 549–549. https://doi.org/10.1017/S0025315400047159

Emani, P. K., & Maheshwari, B. K. (2009). Dynamic impedances of pile groups with embedded caps in homogeneous elastic soils using CIFECM. *Soil Dynamics and Earthquake Engineering*, *29*(6), 963–973. https://doi.org/10.1016/j.soildyn.2008.11.003

Fadiji, T., Coetzee, C. J., Berry, T. M., Ambaw, A., & Opara, U. L. (2018). The efficacy of finite element analysis (FEA) as a design tool for food packaging: A review. *Biosystems Engineering*, *174*, 20–40. https://doi.org/10.1016/j.biosystemseng.2018.06.015\

Fager, E. W. (1964). Marine Sediments: Effects of a Tube-Building Polychaete. *Science*, *143*(3604), 356–359. https://doi.org/10.1126/science.143.3604.356

FEMA P-2091 (2020). *A practical guide to soil-structure interaction*. December (Washington, D.C.: Applied technology council; Federal emergency management agency).

Fukunaga, A. S., Morookian, J. M., Quillin, K., Stoica, A., & Thakoor, S. (1998). *Earthwormlike exploratory robots* (JPL New Technology Report NPS-20266). https://www.techbriefs.com/component/content/article/32180-npo20266

Gans, C. (1973). Locomotion and Burrowing in Limbless Vertebrates. *Nature*, *242*(5397), 414–415. https://doi.org/10.1038/242414a0

Gaymer, R. (1971). New Method of Locomotion in Limbless Terrestrial Vertebrates. *Nature*, *234*(5325), 150–151. https://doi.org/10.1038/234150a0

Ge, J. Z., Calderón, A. A., Chang, L., & Pérez-Arancibia, N. O. (2019). An earthworm-inspired friction-controlled soft robot capable of bidirectional locomotion. *Bioinspiration & Biomimetics*, *14*(3), 036004. https://doi.org/10.1088/1748-3190/aae7bb

Hermans, C. O. (1978). Metamorphosis in the opheliid polychaete Armandia brevis. *Settlement and Metamorphosis of Marine Invertebrate Larvae*, 113–126.

Hill, R. (1950). *The Mathematical Theory of Plasticity*. Clarendon Press.

Jaeger, R. A. (2012). *Numerical and Experimental Study on Cone Penetration in Sands and Intermediate Soils*. [Doctoral dissertation, University of California, Davis]. https://doi.org/10.13140/RG.2.1.2973.9926

Jaeger, R. A. (2018) ASCEND: Applications for Spherical and Cylindrical Cavity Expansion in Nonlinearly Deforming Geomaterials [Unpublished software]. California Department of Water Resources, Division of Safety of Dams

Jain, S., Mishra, P. N., Tiwari, S., Wang, Y., Jiang, N.-J., Dash, H., Chang, I., Kumar, A., Das, S., Scheuermann, A., & Bore, T. (2023). Biological perspectives in geotechnics: Theoretical developments. *Reviews in Environmental Science and Bio/Technology*, *22*. https://doi.org/10.1007/s11157-023-09671-2

Jeong, S. Y., Kang, T. H.-K., Yoon, J. K., & Klemencic, R. (2020). Seismic performance evaluation of a tall building: Practical modeling of surrounding basement structures. *Journal of Building Engineering*, *31*, 101420. https://doi.org/10.1016/j.jobe.2020.101420

Jung, S. (2010). *Caenorhabditis elegans* swimming in a saturated particulate system. *Physics of Fluids*, *22*(3), 031903. https://doi.org/10.1063/1.3359611

Khosravi A., Martinez A., DeJong J.T., and Wilson D. 2018. Discrete element simulations of bio-inspired self-burrowing probes in sands of varying density. In *Proceedings of the Biomediated and Bioinspired Geotechnical (B2G)* Conference, Atlanta, GA, 12–13.

Kier, W. M. (2012). The diversity of hydrostatic skeletons. *Journal of Experimental Biology*, *215*(8), 1247–1257. https://doi.org/10.1242/jeb.056549

Kramer, S. L. (1996). *Geotechnical earthquake engineering*. Prentice Hall.

Kullingsjo A. (2009). Effects of deep excavations in soft clay on the immediate surroundings. In *Proceedings of the 17th International Conference on Soil Mechanics and Geotechnical Engineering*. IOS Press. https://doi.org/10.3233/978-1-60750-031-5-1923

Kurth, J. A., & Kier, W. M. (2014). Scaling of the hydrostatic skeleton in the earthworm *Lumbricus terrestris*. *Journal of Experimental Biology*, *217*(11), 1860–1867. https://doi.org/10.1242/jeb.098137

Kutanis, M. & Elmas, M. (1999). *The Soil Structure Interaction Analysis Based on Substructure Method in Time Domain*. https://www.academia.edu/89817331/The_Soil_Structure_Interaction_Analysis_Based_on_Substructure_Method_in_Time_Domain

Kwag, S., Ju, B., & Jung, W. (2018). Beneficial and Detrimental Effects of Soil-Structure Interaction on Probabilistic Seismic Hazard and Risk of Nuclear Power Plant. *Advances in Civil Engineering*, *2018*(1), 2698319. https://doi.org/10.1155/2018/2698319

Law, C. J., Dorgan, K. M., & Rouse, G. W. (2014). Relating divergence in polychaete musculature to different burrowing behaviors: A study using opheliidae (Annelida). *Journal of Morphology*, *275*(5), 548–571. https://doi.org/10.1002/jmor.20237

Le, C. L., Yirmibesoglu, O. D., Even, S., Buckner, T., Ozkan-Aydin, Y., & Kramer-Bottiglio, R. (2025). Grand challenges for burrowing soft robots. *Frontiers in Robotics and AI, 12,* 1525186. https://doi.org/10.3389/frobt.2025.1525186

Li, G., Qiu, W., Wang, M., Zhu, Y., & Liu, F. (2024). Development of an earthworm-based soft robot for colon sampling. *Frontiers in Robotics and AI*, *11*, 1309220. https://doi.org/10.3389/frobt.2024.1309220

Liu, R., & Yao, Y. (2019). A novel serial–parallel hybrid worm-like robot with multi-mode undulatory locomotion. *Mechanism and Machine Theory*, *137*, 404–431. https://doi.org/10.1016/j.mechmachtheory.2019.03.033

Lou, M., Wang, H., Chen, X., and Zhai, Y. (2011). Structure-soil-structure interaction: Literature review. *Soil Dyn. Earthq. Eng. 31, 1724–1731*. doi:10.1016/j.soildyn.2011.07.008

Manna, B., & Baidya, D. K. (2010). Dynamic nonlinear response of pile foundations under vertical vibration—Theory versus experiment. *Soil Dynamics and Earthquake Engineering*, *30*(6), 456–469. https://doi.org/10.1016/j.soildyn.2010.01.002

Martinez, A., Palumbo, S., & Todd, B. D. (2019). Bioinspiration for Anisotropic Load Transfer at Soil–Structure Interfaces. *Journal of Geotechnical and Geoenvironmental Engineering*, *145*(10), 04019074. https://doi.org/10.1061/(ASCE)GT.1943-5606.0002138

Martinez, A., DeJong, J. T., Jaeger, R. A., & Khosravi, A. (2020). Evaluation of self-penetration potential of a bio-inspired site characterization probe by cavity expansion analysis. *Canadian Geotechnical Journal*, *57*(5), 706–716. https://doi.org/10.1139/cgj-2018-0864

Meyer, J.-A., & Guillot, A. (2008). Biologically Inspired Robots. In B. Siciliano & O. Khatib (Eds.), *Springer Handbook of Robotics* (pp. 1395–1422). Springer Berlin Heidelberg. https://doi.org/10.1007/978-3-540-30301-5_61

Milana, E. (2022). Soft robotics for infrastructure protection. Frontiers in Robotics and AI, 9. https://doi.org/10.3389/frobt.2022.1026891

Mills, A. S. (2025). *Mechanically Compliant Worm-Like Robotics: Exploiting Polymer Properties for Design, Simulation, and Fabrication* [Case Western Reserve University]. https://etd.ohiolink.edu/acprod/odb_etd/etd/r/1501/10?clear=10&p10_accession_num=case1737750362257665

Najar, I. A., Ahmadi, R., Amuda, A. G., Mourad, R., Bendary, N. E., Ismail, I., Bakar, N. A., & Tang, S. (2025). Advancing soil-structure interaction (SSI): A comprehensive review of current practices, challenges, and future directions. *Journal of Infrastructure Preservation and Resilience*, *6*(1), 5. https://doi.org/10.1186/s43065-025-00118-2

Norby, J., Wang, S., Wang, H., Deng, S., Jones, N., Mishra, A., Pavlov, C., He, H., Subramanian, S., Thangavelu, V., Sihota, N., Hoelen, T., Johnson, A. M., & Lowry, G. V. (2024). Path to autonomous soil sampling and analysis by ground-based robots. Journal of Environmental Management, 360, 121130. https://doi.org/10.1016/J.JENVMAN.2024.121130

Pestana, J. M., & Whittle, A. J. (1999). Formulation of a unified constitutive model for clays and sands. *International Journal for Numerical and Analytical Methods in Geomechanics*, *23*(12), 1215–1243. https://doi.org/10.1002/(SICI)1096-9853(199910)23:12%253C1215::AID-NAG29%253E3.0.CO;2-F

Pestana-Nascimento, J. M. (1994). *A unified constitutive model for clays and sands* [Thesis, Massachusetts Institute of Technology]. https://dspace.mit.edu/handle/1721.1/11724

Price, A. B. (2018). *Cyclic Strength and Cone Penetration Resistance for Mixtures of Silica Silt and Kaolin*. [Doctoral dissertation, University of California, Davis].

Purschke, G. & Muller, M. C. (2006). Evolution of body wall musculature. *Integrative and Comparative Biology*, *46*(4), 497–507. https://doi.org/10.1093/icb/icj053

Robertson, P. K. (1990). Soil classification using the cone penetration test. *Canadian Geotechnical Journal*, *27*(1), 151–158. https://doi.org/10.1139/t90-014

Ruiz, S., Or, D., & Schymanski, S. J. (2015). Soil Penetration by Earthworms and Plant Roots—Mechanical Energetics of Bioturbation of Compacted Soils. *PLOS ONE*, *10*(6), e0128914. https://doi.org/10.1371/journal.pone.0128914

Sadava, D., Hillis, D., Heller, H., & Berenbaum, C. (2009). *Life: The Science of Biology, Vol. I*. Macmillan. https://www.abebooks.com/9781429246453/Life-Science-Biology-Vol-Sadava-1429246456/plp

Sadeghi, A., Tonazzini, A., Popova, L., & Mazzolai, B. (2014). A Novel Growing Device Inspired by Plant Root Soil Penetration Behaviors. *PLoS ONE*, *9*(2), e90139. https://doi.org/10.1371/journal.pone.0090139

Saga, N., Tesen, S., Sato, T., & Nagase, J. Y. (2016). Acquisition of earthworm-like movement patterns of many-segmented peristaltic crawling robots. International Journal of Advanced Robotic Systems, 13(5). https://doi.org/10.1177/1729881416657740

Salgado, R., & Prezzi, M. (2007). Computation of Cavity Expansion Pressure and Penetration Resistance in Sands. *International Journal of Geomechanics*, *7*(4), 251–265. https://doi.org/10.1061/(ASCE)1532-3641(2007)7:4(251)

Salgado, R., & Randolph, M. F. (2001). Analysis of Cavity Expansion in Sand. *International Journal of Geomechanics*, *1*(2), 175–192. https://doi.org/10.1061/(ASCE)1532-3641(2001)1:2(175)

Salut to the earthworm robot that can explore other worlds! (2023). CIO Bulletin. https://ciobulletin.com/2023/03/earthworm-robot-used-to-explore-world

Seymour, M. K. (1971). Burrowing behaviour in the European lugworm *Arenicola marina* (Polychaeta: Arenicolidae). *Journal of Zoology*, *164*(1), 93–132. https://doi.org/10.1111/j.1469-7998.1971.tb01299.x

Shin, P. K. S., Ng, A. W. M., & Cheung, R. Y. H. (2002). Burrowing responses of the short-neck clam Ruditapes philippinarum to sediment contaminants. *Marine Pollution Bulletin*, *45*(1–12), 133–139. https://doi.org/10.1016/S0025-326X(01)00299-5

Stewart, J., Crouse, C. B., Hutchinson, T. C., Lizundia, B., Naeim, F., & Ostadan, F. (2012). Soil-Structure Interaction for Building Structures. *NIST*. https://www.nist.gov/publications/soil-structure-interaction-building-structures

Summers, A. P., & O'Reilly, J. C. (1997). A comparative study of locomotion in the caecilians Dermophis mexicanus and Typhlonectes natans (Amphibia: Gymnophiona). *Zoological Journal of the Linnean Society*, *121*(1), 65–76. https://doi.org/10.1111/j.1096-3642.1997.tb00147.x

Tang, Y., & Julian Tao, J. (2021). Effect of Rotation on Penetration: Toward a Seed Awn-Inspired Self-Burrowing Probe. *IFCEE 2021*, 149–159. https://doi.org/10.1061/9780784483428.016

Tang, Y., & Tao, J. (2022). Multiscale analysis of rotational penetration in shallow dry sand and implications for self-burrowing robot design. Acta Geotechnica, 17(10). https://doi.org/10.1007/s11440-022-01492-x

Tang, S., Yao, J., & Yu, Y. (2025). Design and mechanical analysis of a novel modular bionic earthworm robot with upright functionality. Scientific Reports, 15(1), 3829. https://doi.org/10.1038/s41598-025-88235-6

Tang, Y., Zhong, Y., & Tao, J. (2024). Bio-inspired rotational penetration and horizontal self-burrowing soft robot. *Acta Geotechnica*, *19*(3), 1345–1363. https://doi.org/10.1007/s11440-023-02173-z

Trueman, E. R. (1966). Observations On the Burrowing of *Arenicola Marina* (L.). *Journal of Experimental Biology*, *44*(1), 93–118. https://doi.org/10.1242/jeb.44.1.93

Trueman, E. R. (1967). The dynamics of burrowing in *Ensis* (Bivalvia). *Proceedings of the Royal Society of London. Series B. Biological Sciences*, *166*(1005), 459–476. https://doi.org/10.1098/rspb.1967.0007

Tzetlin, A. B., & Filippova, A. V. (2005). Muscular system in polychaetes (Annelida). In T. Bartolomaeus & G. Purschke (Eds.), *Morphology, Molecules, Evolution and Phylogeny in Polychaeta and Related Taxa* (Vol. 179, pp. 113–126). Springer-Verlag. https://doi.org/10.1007/1-4020-3240-4_7

Vesić, A. S. (1972). Expansion of Cavities in Infinite Soil Mass. *Journal of the Soil Mechanics and Foundations Division*, *98*(3), 265–290. https://doi.org/10.1061/JSFEAQ.0001740

Wainwright, S. A. (1988). *Axis and Circumference: The Cylindrical Shape of Plants and Animals*. Harvard University Press. https://doi.org/10.4159/harvard.9780674436961

Wei, H., Zhang, Y., Zhang, T., Guan, Y., Xu, K., Ding, X., & Pang, Y. (2021). Review on Bioinspired Planetary Regolith-Burrowing Robots. *Space Science Reviews*, *217*(8), 87. https://doi.org/10.1007/s11214-021-00863-2

Wells, G. P. (1950). The anatomy of the body wall and appendages in *Arenicola marina* L., *Arenicola claparedii* Levinsen and *Arenicola Ecaudata* Johnston. *Journal of the Marine Biological Association of the United Kingdom*, *29*(1), 1–44. https://doi.org/10.1017/S0025315400056174

Whittle, A. J. (1987). *A constitutive model for overconsolidated clays with application to the cyclic loading of friction piles* [Thesis, Massachusetts Institute of Technology]. https://dspace.mit.edu/handle/1721.1/14639

Winter, A. G., Deits, R. L. H., & Hosoi, A. E. (2012). Localized fluidization burrowing mechanics of *Ensis directus*. *Journal of Experimental Biology*, *215*(12), 2072–2080. https://doi.org/10.1242/jeb.058172

Winter, A. G., V, Deits, R. L. H., Dorsch, D. S., Slocum, A. H., & Hosoi, A. E. (2014). Razor clam to RoboClam: Burrowing drag reduction mechanisms and their robotic adaptation. *Bioinspiration & Biomimetics*, *9*(3), 036009. https://doi.org/10.1088/1748-3182/9/3/036009

Wolf, J. P. (1989). Soil-structure-interaction analysis in time domain. *Nuclear Engineering and Design*, *111*(3), 381–393. https://doi.org/10.1016/0029-5493(89)90249-5

Woodin, S. A. (1974). Polychaete Abundance Patterns in a Marine Soft-Sediment Environment: The Importance of Biological Interactions. *Ecological Monographs*, *44*(2), 171–187. https://doi.org/10.2307/1942310

Yu, H. S., & Houlsby, G. T. (1991). Finite cavity expansion in dilatant soils: Loading analysis. *Géotechnique*, *41*(2), 173–183. https://doi.org/10.1680/geot.1991.41.2.173

Yu, H.-S. (2000). *Cavity Expansion Methods in Geomechanics*. Springer Netherlands. https://doi.org/10.1007/978-94-015-9596-4

Zhang, W., Xiang, J., Huang, R., & Liu, H. (2023). A review of bio-inspired geotechnics-perspectives from geomaterials, geo-components, and drilling & excavation strategies. *Biogeotechnics*, *1*(3), 100025. https://doi.org/10.1016/j.bgtech.2023.100025

Zhao, M., Gao, Z., Wang, L., Du, X., Huang, J., & Li, Y. (2017). Obliquely incident earthquake for soil-structure interaction in layered half space. *Earthquakes and Structures*, *13*(6), 573–588. https://doi.org/10.12989/EAS.2017.13.6.573

Zhidong, G., Xu, Z., Mi, Z., Xiuli, D., Junjie, W., & Pengcheng, L. (2021). Efficient seismic analysis for nonlinear soil-structure interaction with a thick soil layer. *Earthquake Engineering and Engineering Vibration*, *20*(3), 553–565. https://doi.org/10.1007/s11803-021-2038-3